Understanding the thermodynamic effects of chemically reactive working fluids in the Stirling engine

Aya Barakat, Silvia Lasala, Philippe Arpentinier, Pascal Tobaly, Jean-Noël Jaubert

Energy Conversion and Management: X 22 (2024) 100573

Contents lists available at ScienceDirect

Energy Conversion and Management: X

journal homepage: www.sciencedirect.com/journal/energy-conversion-and-management-x

Understanding the thermodynamic effects of chemically reactive working fluids in the Stirling engine

Aya Barakat [a], Silvia Lasala [a,*], Philippe Arpentinier [b], Pascal Tobaly [c], Jean-Noël Jaubert [a]

[a] Université de Lorraine, CNRS, LRGP, F-54000 Nancy, France
[b] Air Liquide, Innovation Campus Paris, 1 chemin de la porte des loges, 78354 Jouy-en-Josas, France
[c] Lafset (Laboratoire du froid et des systèmes énergétiques et thermiques), CNAM, HESAM Université, 292, rue Saint-Martin, Paris 75003, France

ARTICLE INFO

Keywords:
Stirling engine
Energy efficiency
Working fluid
Chemically reactive gas
Thermodynamic analysis
Chemical equilibrium
Applications

ABSTRACT

The Stirling engine, renowned for its high theoretical efficiency, is capable of partaking an active role in the current energy transition. Given its closed-cycle operation, the choice of the working fluid is pivotal in designing the Stirling engine. Dinitrogen tetroxide (N_2O_4) has been extensively investigated in the past, based on the ideal gas thermodynamic model, as a chemically reactive working fluid for Stirling cycles. This molecule reversibly and rapidly dissociates into nitrogen dioxide (NO_2)–and recombines into N_2O_4–under the influence of thermodynamic transformations throughout the cycle, in accordance with chemical equilibrium. Addressing discrepancies in previous studies, this work aims at assessing a wide range of theoretical chemically reactive gases as working fluids in a Stirling cycle, employing the ideal gas mixture model. The behavior of each reactive fluid is examined throughout the cycle, and the thermodynamic performance is evaluated. Therefore, this work quantifies and analyzes the thermodynamic performance of a chemically reactive Stirling engine. Results indicate a slight increase in the net specific work output with certain reactive fluids, offering a thermal efficiency comparable to that of inert working fluids. In addition, it is emphasized that for chemically reactive working fluids, the isochoric heat exchange within the internal regenerator is incomplete due to chemical reactions, in contrast to the case of inert fluids. To address this, either a supplementary heat source, heat sink, or both are required during the isochoric processes. Furthermore, chemically reactive fluids in the Stirling engine induce irreversibility in the internal regenerator, stemming from heat exchange across a finite temperature difference, penalizing the thermal efficiency of the engine for the majority of reactive fluids studied.

1. Introduction

1.1. The Stirling engine

As it has become critical to shift to greener energy sources and more efficient energy converters, the Stirling engine has been gaining desirability due to the role that it can partake in the current energy transition [1,2].

This engine precedes the development of both the Carnot and internal combustion engines. Initially designed to operate on a closed regenerative thermodynamic cycle with a gaseous working fluid, it offers flexibility in utilizing a variety of environmentally friendly energy sources.

The Stirling cycle is characterized by a sequence of four thermodynamic transformations in theory. These include isothermal expansion, where thermal energy is introduced and work is generated as the fluid expands; internal isochoric cooling, where the fluid is cooled in an internal regenerator; isothermal compression, where thermal energy is released to the heat sink and the fluid is compressed by the input compression work; and internal isochoric heating, where the fluid is internally heated in the regenerator using the thermal energy extracted during the internal isochoric cooling process. It can be demonstrated that this ideal cycle–assumed internally reversible–is characterized by a high first-law efficiency, equivalent to the Carnot efficiency.

1.2. Applications

Due to the system's aforementioned advantages, in addition to its ease of maintenance and silent mode of operation, the Stirling engine has found various applications. Operating on the direct Stirling cycle,

* Corresponding author.
E-mail address: silvia.lasala@univ-lorraine.fr (S. Lasala).

https://doi.org/10.1016/j.ecmx.2024.100573
Received 19 January 2024; Received in revised form 4 March 2024; Accepted 16 March 2024
Available online 19 March 2024

the engine can serve as a prime mover in automotive, marine, and aerospace applications, as well as in mechanical–electrical energy conversion. Alternatively, operating on the reverse Stirling cycle, the system can be implemented in cooling–especially cryogenic–and heating applications, converting mechanical power into thermal power.

1.2.1. The Stirling cycle

Operating on its direct cycle, the Stirling engine generates mechanical work by harnessing a high-quality heat source. This mechanical work output could be directly valorized for mechanical propulsion or drive, or the Stirling machine could be coupled to an electric generator to produce electric power. The energy source fueling the Stirling engine could be a combustor, solar thermal energy [3], radioisotope, electric resistance, or thermal energy storage. Furthermore, Stirling engines could be utilized as bottoming cycles in waste heat recovery applications [4,5].

1.2.1.1. Mechanical propulsion and drive. Utilizing the Stirling machine as an automotive engine in conventional powertrains–rather than the internal combustion engine (ICE)–has been the focus of several studies. The interest grew due to the engine's improved thermal efficiency and higher torque at low engine speeds, compared to the conventional ICE [6]. Indeed, Stirling engine vehicles gained momentum in the 70's and 80's as several prototypes were developed and tested including the 4-98 [7] and 4-215 [8] Ford engines, MOD I [9], MOD II [6], and General Motors GPU-3 [10] engines. These studies showed improved fuel economy and reduced vehicle emissions [6]. However, the interest in this powertrain declined due to the deficient power density, production cost, control difficulty, long start-up time, and, mainly, the competitiveness of the ICE. Nonetheless, the resurgence of series hybrid powertrains in the early 2000s presented an opportunity to utilize the Stirling engine as an energy converter in the auxiliary power unit (APU), where the engine operates at a quasi-steady high-efficiency state and is decoupled from the drivetrain. The Stirling engine is, thus, coupled to an electric generator that feeds the vehicle's battery, according to the command of the APU controller. Ghanem et al. compared the performance and fuel consumption of a regenerative reheat two-stage Stirling machine APU and a conventional ICE-APU in a series hybrid electric vehicle model [11]. Results show a reduction in the fuel consumption of the Stirling-APU by 12 % compared to the ICE-APU. Furthermore, the optimal thermal efficiency of the selected Stirling configuration amounted to 41 % compared to 36 % corresponding to an ICE. However, a 38 % reduction in the system's net specific work output is observed. Similarly, Bou Nader et al. investigated the potential fuel savings of a series–parallel hybrid electric powertrain with a Stirling machine as the energy converter [12]. Consequently, the authors simulated a regenerative MOD II Stirling machine–with a maximum efficiency of 38.5 %–in a Toyota Prius powertrain, and results show 3.5 % to 5.5 % improvement in fuel consumption compared to a similar ICE configuration.

On the other hand, Stirling engines have proven to be attractive pertaining to marine applications. For instance, the Swedish Navy's Gotland-class, and the preceding Södermanland-class, submarines employ an air-independent Stirling engine–produced by Kockums–that operates on the combustion of diesel, given the availability of on-board liquid oxygen [13]. Indeed, the implementation of the Stirling engine in submarines has increased their underwater endurance to around two weeks, an unmatched endurance that has not been achieved except in nuclear-powered submarines.

As for aerospace applications, deep space missions require resilient energy converters that do not need regular maintenance; these are characteristics of the Stirling engine. A recent NASA demonstration proved that a free-piston Stirling engine is capable of achieving a 14-year maintenance-free successful operation [14,15]. The engine is powered by a decaying radioisotope and is part of NASA's dynamic radioisotope power systems (RPS) project. Furthermore, its expected best converter efficiency amounts to 21 %. In addition, the China National Space Agency (CNSA) announced the completion of the first in-orbit test of a Stirling engine as part of the Shenzhou-15 mission in 2023 [16]. Therefore, the Stirling engine is expected to play a significant role in the future of space exploration.

1.2.1.2. Electricity generation. As in the case of hybrid electric vehicles and submarines, the Stirling engine could be coupled to an electric generator in order to convert the mechanical power output into electricity in stationary applications. In the case of solar-powered Stirling engines [17], the Stirling machine is coupled to a parabolic solar concentrator and generates mechanical power output. In turn, this mechanical power is converted to electricity by means of a generator. In fact, the Maricopa power plant (first commercial solar-powered Stirling power plant deploying the SunCatcher technology) in Arizona, USA consisted of 60 dishes, each connected to a generator producing an electric power of 25 kW [18]. Therefore, the powerplant produced 1.5 MW of electricity. These systems have demonstrated high solar-to-electricity net efficiency. Additionally, the thermal efficiency of the Stirling engine in the system could reach about 34 % [19]. The plant decommissioned in 2011 due to issues with the supply of Stirling engine components and a lack of technological readiness.

Another application to the Stirling engine is cogeneration where the engine generates electricity and useful heat mainly for low-temperature applications. A gas-fired SOLO V161 micro-CHP (combined heat and power) achieves an overall efficiency in the range of 88.84 %–92 % [20]. Furthermore, the diesel-fired WhisperGen DC system achieves an overall energy efficiency of 90.5 % [21].

1.2.2. The reverse Stirling cycle

Alternatively, operating on its reverse cycle, the Stirling system could be utilized to produce a cooling (Stirling cryocooler or refrigerator) or heating (Stirling heat pump) effect.

1.2.2.1. Stirling cryocooler. One of the most common applications to the reverse Stirling system is cryogenics. This is due to the system's ability to reach low temperatures robustly when mechanical work is provided to the system [22], permitting the liquification of hydrogen (20 K) and helium (4 K), in example. Stirling cryocoolers are being extensively used for gas liquification, cryopumping, and military applications [23]. Indeed, the Stirling cryocooler proves to be competitive to other cryogenic technologies, achieving an efficiency of 30 % relative to the theoretical Carnot performance at 77 K and 650 W cooling capacity [24]. In another experimental study, a relative-to-the-Carnot efficiency of 26.8 % was achieved at 80 K and 350 W cooling capacity for a free piston Stirling system [25].

1.2.2.2. Stirling heat pump. On the other hand, Walker provided a preliminary estimate for the Stirling heat pump's actual coefficient of performance, amounting to approximately two for a well-designed system [23]. However, in an experimental investigation of a beta-type Stirling machine, a coefficient of performance (COP) of 3.5 was achieved with an output temperature of 374 K and air as the working fluid [26]. Note that the COP of a typical air-source residential heat pump, which operates on the vapor compression cycle, ranges from 2 to 4. In reality, Stirling heat pumps suffered several challenges that prevented their commercialization: thermal and mechanical losses, high cost of production, working fluids leakage, and challenging system control. Nonetheless, with the development of the free piston Stirling machine [27], the problem of fluid leakage has been tackled. Furthermore, the Stirling heat pump proves to be more eco-friendly and yields lower exergy losses over its lifetime compared to other heating technologies [28]. Therefore, the Stirling heat pump is expected to play a vital role in the future heating industry, especially in the light of emission-reduction regulations and anticipated technological advancements of the system.

1.3. Working fluids

1.3.1. Inert working fluids

Since the Stirling engine operates on a closed cycle, the choice of a working fluid is of utter importance. To date, the most commonly used working fluids are air, helium, and hydrogen gases due to their thermodynamic and transport properties including high specific heat capacity, high thermal conductivity, and low viscosity [29]. Although the initial design of the Stirling engine was based on gaseous working fluids, liquid and composite working fluids have been investigated. Swift compared the performance of a liquid Stirling engine (propylene) to that of a Rankine cycle in a refrigeration application [30]. Both theoretical and experimental results demonstrate a very close performance (measured by the ratio of the COP to the COP of a Carnot cycle) between the highly developed Rankine system and a laboratory-scale, unoptimized Stirling cycle. Specifically, the theoretical efficiency of the studied Stirling cycle amounted to 70 %, whereas the experimental efficiency was limited to 20 %. In addition, the Malone engine, a modified version of the Stirling engine that operates with a liquid working fluid, and that dates back to the 1920s, has been investigated [31,32]. On the other hand, Walker demonstrated that two-phase two-component working fluids for cryogenic Stirling engines may allow for significant improvement in refrigerating capacity [33]. These fluids are comprised of a gaseous carrier and a phase-changing component that is liquid in the engine's cold compartment and gas in the hot counterpart (also referred to as compound fluids). Subsequently, Renfroe assessed two-phase two-component working fluids for Stirling engines by adding water to air [34,35]. Results show a 150 % increase in the power output, confirming the predictions made by Walker.

1.3.2. Chemically reactive working fluids

Other unconventional working fluids have been investigated in pursuit of enhancing the engine's power output and efficiency. These are referred to as chemically reactive working fluids that undergo chemical reactions under the influence of thermodynamic transformations in the cycle, including changes in temperature and pressure [36]. Therefore, these fluids are based on equilibrated chemical reactions where the chemical equilibrium shifts to accommodate changes in the thermodynamic state of the fluid, altering the fluid's equilibrium composition. In his thesis, Wolgemuth investigated the use of chemically reactive gases as working fluids in a Stirling cycle [37]. His work specifically focused on the use of dinitrogen tetroxide that is based on the equilibrated equation $N_2O_4 \rightleftarrows 2\ NO_2 \rightleftarrows 2\ NO + O_2$ (in the gaseous phase). A significant increase in the net work per unit maximum cylinder volume was obtained compared to the use of inert fluids. However, this was offset by a slight decrease in the thermal efficiency. This is due to the incomplete internal heat exchange in the regenerator during the isochoric processes when using reactive dinitrogen tetroxide, meaning that the heat rejected during the isochoric cooling process is not equivalent to the heat absorbed during the isochoric heating process. Specifically, for the studied reactive fluid, the heat rejected during isochoric cooling, for the different operating conditions considered by Wolgemuth, was found to be always higher than that needed during the isochoric heating process. As explained by Wolgemuth, the reason for the difference between these two heat quantities is the difference in pressures between these two processes, and this has an effect on the fluid's composition for the case of reactive working fluids. Therefore, the surplus heat released during isochoric cooling is rejected out of the cycle, and this causes a loss in thermal efficiency. Similarly, using the Schmidt analysis [38], Walker assessed using N_2O_4 as a chemically reactive working fluid in a Stirling engine with the presence of an inert gaseous carrier [29]. Results show a possible substantial increase in the net specific work output of the engine without size, weight, or cost penalties, compared to non-reacting gaseous working fluids. In a subsequent book, Walker supplemented his earlier conclusion regarding the advantages of utilizing a chemically reactive working fluid in a Stirling engine, based on a "very limited and highly idealized study", by concluding that these fluids offered no significant advantages compared to the inert two-phase two-component working fluids [39]. Precedingly, in the Union of Soviet Socialist Republics (USSR), Kovtun et al. investigated the use of chemically reactive gases in an ideal Stirling engine and demonstrated that an effective efficiency of 24 % could be achieved, compared to 13 % which corresponds to an inert gas cycle [40]. The authors based their analysis on the fact that the heat added and rejected during the isochoric processes is carried out externally–rather than within an internal regenerator.

Based on the reviewed literature, it is evident that the exploration of reactive working fluids for Stirling engines has been limited to N_2O_4. However, this fluid poses toxicity and corrosion problems, limiting its use for real applications. Therefore, in order to leverage the benefits of reactive working fluids, it is essential to identify and investigate alternative fluid options. In addition, theoretical analysis reveals that, in N_2O_4-based Stirling engines, the heat exchanged during the two isochoric processes is not completely carried out internally in the regenerator, contrary to Stirling cycles operating with inert fluids. Consequently, the conclusions of previous studies are not in line due to the differences in the thermodynamic methodologies followed, given the reactive engine's additional degree of freedom: the incomplete internal regeneration.

Hence, this work is aimed to study the effect of utilizing chemically reactive gases as working fluids in the Stirling cycle, following a thermodynamic methodology previously adopted by the authors in their investigations of reactive Brayton power cycles [41] and heat pumps [42]. This approach includes assessing a range of theoretical gaseous reactive fluids, each characterized by a unique set of reaction coordinates: standard entropy and enthalpy change of reaction. These gases are modeled as ideal gas mixtures that evolve throughout the cycle, based on the respective equilibrated chemical reactions. The behavior of the reactive gas is assessed in each of the Stirling cycle's units and–whenever possible–benchmarked against that of comparable inert gases. In addition, the cycle's performance, quantified by the specific net work output and thermal efficiency, is investigated for the spectrum of reactive fluids considered.

2. Methodology

This section presents the methodology followed in this work and introduces: the studied Stirling engine cycle (Section 2.1), the path followed to model the theoretical gaseous mixtures (Section 2.2), and the thermodynamic approach (Section 2.3) for evaluating the engine's performance.

2.1. The Stirling cycle

The Stirling engine is a reciprocating regenerative thermal engine that typically operates with a gaseous working fluid. It follows the Stirling thermodynamic cycle, which consists of four processes: (1–2) isothermal expansion, (2–3) isochoric cooling, (3–4) isothermal compression, and (4–1) isochoric heating. The sequence of these processes is schematically depicted in Fig. 1(a). Fig. 1(b) presents a pressure–volume (P-v) diagram of the ideal Stirling cycle operating with an inert ideal gas as the working fluid. The specific heat and work quantities exchanged are also indicated.

Therefore, the Stirling engine is characterized by a closed thermodynamic cycle where the same amount of working fluid is alternatively compressed and expanded in the cold and hot compartments of the engine, respectively, as depicted in Fig. 1(a). What distinguishes the Stirling engine from other energy converters is the internal regenerator which is usually made of a metallic mesh [43] and exchanges heat with the fluid. Therefore, it acts as an internal heat exchanger, storing heat from the fluid after the isothermal expansion process and releasing it to the fluid after isothermal compression.

Ideally, a Stirling engine operating with an inert perfect gas achieves

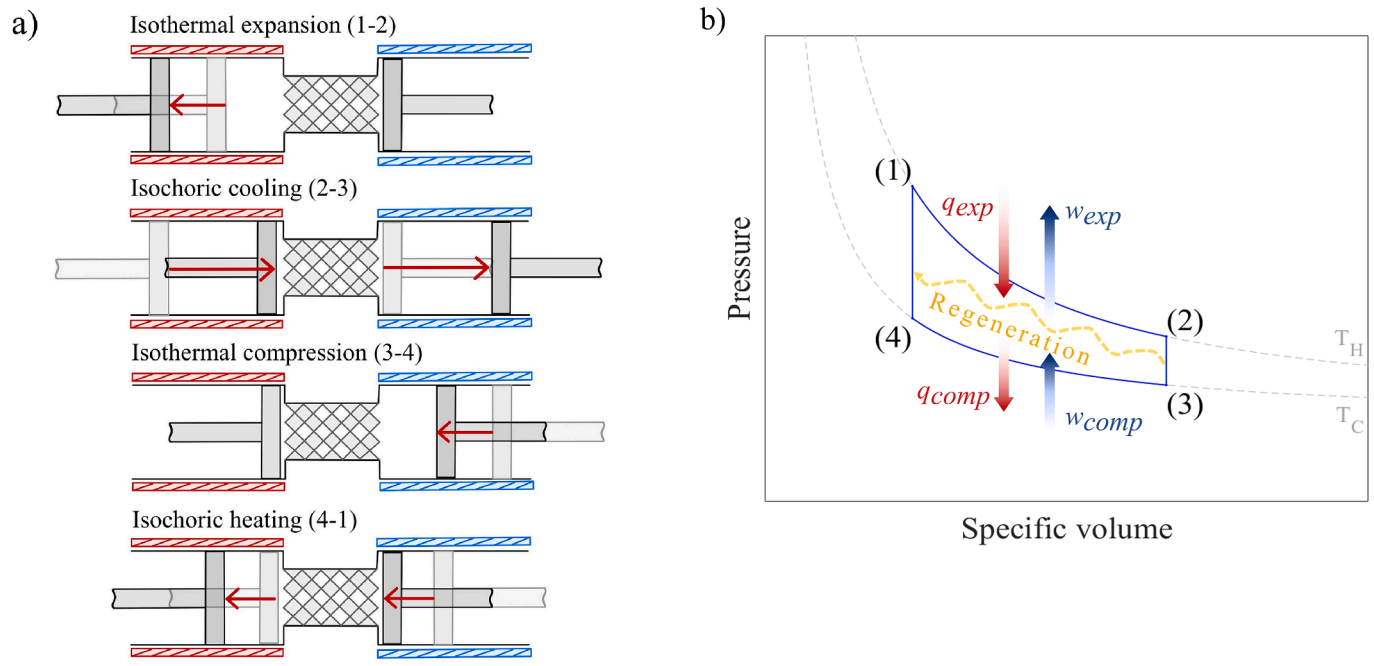

Fig.1. (a) A schematic of the Stirling engine's four processes. (b) P-v diagram of the ideal Stirling cycle operating with an inert ideal gas.

a first-law efficiency that is equivalent to the Carnot efficiency. In the regenerator, the heat released during isochoric cooling is balanced by that absorbed during isochoric heating, and this heat exchange is reversible. Therefore, external heat transfer exclusively takes place during isothermal expansion and compression. However, the utilization of chemically reactive working fluids leads to more complicated thermodynamic analysis, as detailed in Section 2.3.

Therefore, in this study the following assumptions are adopted:

- The engine operates with an ideal gas or gaseous mixture.
- There are no internal losses in the engine, including leakage, friction, and mechanical losses.
- The expansion and compression processes occur at constant temperatures, respectively T_H and T_C:

$$\begin{cases} T_1 = T_2 = T_H \\ T_3 = T_4 = T_C \end{cases} \quad (1)$$

- Processes (2–3) and (4–1) take place at constant volumes.

Note that in the case of incomplete regeneration in the reactive Stirling engine, the heat rejection during isochoric process (2–3) and/or heat gain during isochoric process (4–1) is not completely internal; a portion of the heat is externally transferred, as discussed in Section 2.3.

2.2. Modeling of reactive working fluids

In this study, a range of theoretical reactive ideal gas mixtures is assessed as the working fluids for the Stirling engine. Each of these fluids is based on an equilibrated chemical reaction that is identified by a specific value of the standard entropy change of reaction $\Delta_R S^\circ$ and standard enthalpy change of reaction $\Delta_R H^\circ$. In other words, each set of these parameters $(\Delta_R S^\circ, \Delta_R H^\circ)$ indicates a unique reactive ideal gas mixture, corresponding to a unique chemical reaction. Therefore, as the thermodynamic state of the working fluid changes throughout the Stirling cycle, the chemical equilibrium shifts instantaneously in either direction of the reaction, leading to a new equilibrium state and molar composition. For reference, a similar methodology to assess reactive fluids in other thermodynamic cycles has been adopted in previous publications by the authors [41,42].

Hence, each theoretical reactive fluid is represented by the following equilibrated chemical reaction between the theoretical chemical species A and its dimer A_2, so that A and A_2 compose the ideal gas mixture throughout the cycle:

$$A_{2(g)} \rightleftarrows 2A_{(g)} \quad (2)$$

The forward reaction $A_{2(g)} \rightarrow 2A_{(g)}$ represents a dissociation reaction whereas the reverse reaction $2A_{(g)} \rightarrow A_{2(g)}$ represents an association/recombination reaction. For any thermodynamic state, the molar mass of the gaseous mixture at equilibrium can be calculated using Eq. (3) below:

$$M = z_{A_2} \cdot M_{A_2} + z_A \cdot M_A \quad (3)$$

Where z_{A_2} and z_A are the molar fractions, and M_{A_2} and M_A are the molar masses of molecules A_2 and A, respectively. Note that the molar mass of A is considered 1 g/mol.

The constant-pressure molar heat capacities of the ideal gases present in the reactive mixture, C_{p,A_2} and $C_{p,A}$, are evaluated using the equipartition theorem [44]. In particular, the theorem implies that for monoatomic molecules, the molar heat capacity can be expressed as $C_{p,A} = (5/2)R$, and for diatomic molecules, it can be expressed as $C_{p,A_2} = (7/2)R$, where R is the ideal gas constant. Therefore, the molar mass, heat capacities of the individual ideal gases, and equilibrium composition of the working fluid will be used to evaluate the thermodynamic properties throughout the cycle, as detailed in Section 2.3.

The ranges of the reaction coordinates $(\Delta_R S^\circ, \Delta_R H^\circ)$ that are considered in this study refer to typical chemical reactions' standard entropy change of reaction $\Delta_R S^\circ$ (0 to 0.2 kJ/mol K) and standard enthalpy change of reaction $\Delta_R H^\circ$ (0 to 150 kJ/mol) [41,42]. The positive sign of these coordinates refers to the forward direction of the reaction in Eq. (2). Note that the dissociation reaction $A_{2(g)} \rightarrow 2A_{(g)}$ is endothermic whereas the reverse association reaction is exothermic.

2.3. Thermodynamic analysis

In order to evaluate the thermodynamic properties of the working fluid throughout the Stirling cycle, the fluid's equilibrium composition–influenced by the operating conditions–should be evaluated.

The condition for chemical equilibrium can be expressed as [45]:

$$\Delta_R G \overset{chemical\ equilibrium}{=} 0 \tag{4}$$

Where $\Delta_R G$ is the Gibbs energy change of reaction. The latter can be expressed in terms of the stoichiometric number υ_i and chemical potential μ_i of species i in the gaseous mixture as per the equation below:

$$\Delta_R G = \sum_i \upsilon_i \mu_i \tag{5}$$

The chemical potential μ_i of an ideal gas i in a mixture can be expressed as:

$$\mu_i(T,P) = \mu_i^\circ + RT\ln\left(\frac{P_i}{P^\circ}\right) \tag{6}$$

Where μ_i° is the standard chemical potential of ideal gas i (i.e. its chemical potential at the standard pressure ($P^\circ = 1$ bar) and reference temperature $T_0 = 25^\circ C$) and P_i is its corresponding partial pressure ($P_i = z_i P$).

Substituting Eq. (6) in Eq. (5), the latter becomes:

$$\Delta_R G = \Delta_R G^\circ + RT\ln \mathrm{P} \text{ with } \mathrm{P} = \prod_i \left(\frac{P_i}{P^\circ}\right)^{\upsilon_i} \tag{7}$$

Where, the standard Gibbs energy change of reaction is given by $\Delta_R G^\circ = \sum_i \upsilon_i \mu_i^\circ$.

By definition, the equilibrium constant K is given by:

$$K \equiv \exp\left(\frac{-\Delta_R G^\circ}{RT}\right) = \exp\left(\frac{-\sum_i \upsilon_i \mu_i^\circ}{RT}\right) \tag{8}$$

Hence, combining Eqs. (4), (7), and (8), K can be expressed as:

$$K = \mathrm{P}_{eq} = \prod_i \left(z_i \frac{P}{P^\circ}\right)^{\upsilon_i} \tag{9}$$

The stoichiometric numbers of A_2 and A can be deduced from the chemical reaction presented in Eq. (2) ($\upsilon_{A_2} = -1$, $\upsilon_A = 2$), and the molar fraction of species i can be written in terms of the number of moles n_i and the total number of moles in the system n_{tot} as $z_i = n_i/n_{tot}$.

On the other hand, the number of moles n_i can be written as a function of the initial number of moles $n_{i,0}$, the stoichiometric number υ_i, and the extent of reaction ξ as follows:

$$n_i = n_{i,0} + \upsilon_i \xi \tag{10}$$

Therefore, starting from Eq. (9), K can be expressed as a function of the system's equilibrium pressure P, extent of reaction at equilibrium ξ, and initial number of moles ($n_{A_2,0}$, $n_{A,0}$):

$$K = \frac{P/P^\circ}{n_{A_2,0} + n_{A,0} + \xi} \cdot \frac{\left(n_{A,0} + 2\xi\right)^2}{n_{A_2,0} - \xi} \tag{11}$$

Furthermore, K can be evaluated using the system's temperature T and the reaction coordinates ($\Delta_R S^\circ, \Delta_R H^\circ$) taken at a reference temperature (T_0), according to the Ulich approximation [42,45]:

$$\ln K(T) = \frac{\Delta_R S^\circ(T_0)}{R} - \frac{\Delta_R H^\circ(T_0)}{RT} \tag{12}$$

Therefore, for a chemically reactive working fluid–identified by the reaction coordinates ($\Delta_R S^\circ, \Delta_R H^\circ$)–the equilibrium constant K can be evaluated according to Eq. (12), knowing the system's temperature T. Subsequently, given the stoichiometry of the chemical reaction presented in Eq. (2), the initial number of moles of A_2 and A, and the system's pressure P, the extent of reaction ξ can be calculated using Eq. (11). Hence, the equilibrium composition of the ideal gas mixture (number of moles and molar fraction) can be calculated using ξ, as presented in Eq. (10).

Starting from the equilibrium composition at each (T,P) condition in the cycle, other thermodynamic properties can be evaluated using the equations in Table 1, according to the ideal gas mixture model [45,46].

In this study, the value of the initial number of moles of A_2 and A are considered $n_{A_2,0} = 1$ mol and $n_{A,0} = 0$ mol, respectively. Therefore, the equations for the extent of reaction ξ, molar mass M, and other thermodynamic properties of the gaseous mixture can be derived, as presented in Table 2.

Therefore, for any isochoric process (i - ii), where T_i, P_i, and T_{ii} are known, P_{ii} can be calculated by solving Eq. (23), knowing that v is given by Eq. (22), and ξ is a function of T and P–as presented in Eq. (18).

$$v_i(T_i, P_i) = v_{ii}(T_{ii}, P_{ii}) \tag{23}$$

The system's lowest and highest pressures (P_3 and P_1), as well as the cycle temperatures (T_H and T_C), are given (refer to Fig. 1). Considering Eq. (23), the unknown pressures, P_2 and P_4, can be calculated by solving the system of equations below.

Table 1
Thermodynamic properties of an ideal gas mixture.

Thermodynamic property of an ideal gas mixture	Equation	
Specific internal energy, u[kJ/g]	$u(T,\vec{z}) = \frac{\sum_i z_i U_i(T)}{M}$	(13)
	$U_i(T) = U_i^\circ(T_0) + C_{v,i}(T - T_0)$	(14)
	Where, M: molar mass of the gaseous mixture at equilibrium given by Eq. (3) $U_i(T)$: molar internal energy of pure ideal gas i $U_i^\circ(T_0)$: standard molar internal energy of pure ideal gas i at the reference temperature T_0 Recall that: $U_i^\circ(T_0) = \Delta_f H_i^\circ(T_0) - RT_0$, where $\Delta_f H_i^\circ(T_0)$ is the standard molar enthalpy change of formation of pure ideal gas i By definition, the standard enthalpy change of reaction is given by: $\Delta_R H^\circ(T_0) = \sum_i \upsilon_i \Delta_f H_i^\circ$ $C_{v,i}$: constant-volume molar heat capacity of pure ideal gas i that can be evaluated as: $C_{v,A_k} = C_{p,A_k} - R = \begin{cases} 3/2R \text{ for } k=1 \\ 5/2R \text{ for } k=2 \end{cases}$ Note that in this study, the standard molar enthalpy change of formation of A_2 is assumed to be 0 kJ/mol.	
Specific entropy, s[kJ/g]	$s(T,P,\vec{z}) = \frac{\sum_i z_i [S_i(T,P) - R\ln z_i]}{M}$	(15)
	$S_i(T,P) = S_i^\circ(T_0) + C_{p,i}\ln\frac{T}{T_0} - R\ln\frac{P}{P^\circ}$	(16)
	Where, $S_i(T,P)$: molar entropy of pure ideal gas i $S_i^\circ(T_0)$: standard molar entropy of pure ideal gas i at P° and reference temperature T_0 Recall that, by definition, the standard entropy change of reaction is given by: $\Delta_R S^\circ(T_0) = \sum_i \upsilon_i S_i^\circ(T_0)$ Note that in this study, the standard molar entropy of A_2 is assumed to be 0 kJ/mol K.	
Specific volume, v[m^3/g]	$v(T,P,\vec{z}) = \frac{RT}{MP}$	(17)

Table 2
Thermodynamic properties of a chemically reactive ideal gas mixture of A_2 and A, $A_{2(g)} \rightleftarrows 2A_{(g)}$.

Property of the ideal gas mixture $A_{2(g)} \rightleftarrows 2A_{(g)}$	Equation *for each set of the reaction coordinates* $(\Delta_R S^\circ, \Delta_R H^\circ)$	
Extent of reaction at equilibrium, ξ[mol]	$\xi(T,P) = \sqrt{\frac{K}{4P/P^\circ + K}}$ Where, K can be calculated as a function of T using Eq. (12)	(18)
Molar mass, M[g/mol]	$M(T,P) = \frac{2}{1+\xi}$ Note that $z_A = \frac{2\xi}{1+\xi}$ and $z_{A_2} = \frac{1-\xi}{1+\xi}$	(19)
Specific internal energy, u[kJ/g]	$u(T,P) = \xi U_A{}^\circ + \frac{1-\xi}{2} U_{A_2}{}^\circ + \frac{5+\xi}{4} R(T - T_0)$	(20)
Specific entropy, s[kJ/g]	$s(T,P) = \xi S_A{}^\circ + \frac{1-\xi}{2} S_{A_2}{}^\circ + \frac{7+3\xi}{4} R \ln \frac{T}{T_0}$ $-\frac{1+\xi}{2} R \ln \frac{P}{P^\circ} - R\left(\xi \ln \frac{2\xi}{1+\xi} + \frac{1-\xi}{2} \ln \frac{1-\xi}{1+\xi}\right)$	(21)
Specific volume, $v[\mathrm{m^3/g}]$	$v(T,P) = \frac{RT}{2P}(1+\xi)$	(22)

$$\begin{cases} v_2 = v_3 \\ v_4 = v_1 \end{cases} \tag{24}$$

After solving for the unknown pressures, the thermodynamic properties at each state in the cycle can be calculated using the equations in Table 2. Consequently, the heat and work quantities, as well as the system's overall performance, can be evaluated.

The heat input during isothermal expansion $\left(q_{exp}\right)$, as well as the heat rejected $\left(q_{comp}\right)$ during isothermal compression, are calculated according to Eqs. (25) and (26), respectively.

$$q_{exp} = T_H(s_2 - s_1) \tag{25}$$

$$q_{comp} = T_C(s_3 - s_4) \tag{26}$$

The system's net specific work output w_{net} can be evaluated using Eq. (27).

$$w_{net} = w_{exp} - w_{comp} \tag{27}$$

Where w_{exp} is the expansion specific work generated, and w_{comp} is the compression specific work input, calculated as follows:

$$w_{exp} = u_1 - u_2 + q_{exp} \tag{28}$$

$$w_{comp} = u_4 - u_3 + q_{comp} \tag{29}$$

The total heat released during isochoric cooling (2–3), as well as the total heat absorbed during isochoric heating (4–1), are given by the equations below:

$$q_{23} = u_2 - u_3 \tag{30}$$

$$q_{41} = u_1 - u_4 \tag{31}$$

In the case of reactive working fluids, in line with previous research, the heat exchange during isochoric processes in the internal regenerator is incomplete. This can be attributed to the impact of the fluid's reactivity on its specific heat capacity, deviating from the inert ideal isothermal heat transfer. Three cases can result from incomplete regeneration in a reactive Stirling engine as listed below.

- For some reactive fluids, during isochoric cooling (2–3), part of the heat released is stored in the internal regenerator $\left(q_{reg}\right)$ while the rest of the heat–that is not useful for regeneration–is rejected out of the cycle $\left(q_{rej}\right)$. An additional heat sink between thermodynamic states (2) and (3) is needed. The heat stored during (2–3) is sufficient to heat the stream entering the regenerator during isochoric heating (4–1).

$$\begin{cases} q_{23} = q_{reg} + q_{rej} \\ q_{41} = q_{reg} \end{cases}$$

- For other reactive fluids, during isochoric heating (4–1), part of the absorbed heat comes from the internal regenerator $\left(q_{reg}\right)$ while the rest is input via an additional external heat source (q_{add}). The heat stored in the regenerator is not enough to heat the stream during (4–1). Furthermore, the heat rejected during (2–3) is fully stored in the internal regenerator (completely useful for regeneration).

$$\begin{cases} q_{23} = q_{reg} \\ q_{41} = q_{reg} + q_{add} \end{cases}$$

- For the rest of reactive fluids, part of the heat released during (2–3) is stored in the regenerator $\left(q_{reg}\right)$ while the rest is expelled out of the cycle $\left(q_{rej}\right)$. The stored heat, however, is not enough to heat the stream entering the regenerator during (4–1). Hence, part of the heat absorbed during (4–1) comes from the internal regenerator $\left(q_{reg}\right)$ while the rest comes from an external heat source (q_{add}). In this case, an additional heat sink and source are both needed in the cycle as a result of the fluid's reactivity.

$$\begin{cases} q_{23} = q_{reg} + q_{rej} \\ q_{41} = q_{reg} + q_{add} \end{cases}$$

The condition for determining whether the heat released during isochoric cooling (2–3) is useful for regeneration is as follows: for each increment of q_{23} released into the regenerator, the temperature of the hot stream (2–3) must be greater than or equal to that along (4–1) which results from absorbing the same quantity of heat. In other words, in a temperature-heat (T-q) diagram of the regenerator streams, the minimum pinch point temperature difference between the two streams should be greater than or equal to zero. That is the criterion for calculating q_{reg}, which is a fraction of, or equal to, the total heat released during isochoric cooling (q_{23}).

Therefore, the equation of the thermal efficiency η should account for any supplementary heat addition, if applicable, during isochoric heating (4–1), as presented in Eq. (32).

$$\eta = \begin{cases} \dfrac{w_{net}}{q_{exp}} & \text{for } q_{41} \leqslant q_{reg} \\ \dfrac{w_{net}}{q_{exp} + q_{add}} & \text{for } q_{41} > q_{reg} \end{cases} \quad (32)$$

The thermodynamic assessment is performed for the operating conditions: $P_3 = 0.1$ bar, $T_H = 900$ K, and $T_C = 400$ K. Indeed, the choice of the operating conditions is strictly constrained by the ideal gas assumption adopted in this study. The assumption dictates low pressure values, and that the maximum slope in the P-v diagram of the cycle, namely the slope $\left(\frac{dP}{dv}\right)_{T_1,v_1}$ at thermodynamic point (1), should reflect the behavior of an ideal gas. Therefore, an absolute limit of this slope ($a_{max} = 50$) has been set based on typical values for real gases [47]:

$$\left|\left(\frac{dP}{dv}\right)_{T_1,v_1}\right| < a_{max} \quad (33)$$

Therefore, the lowest pressure (P_3) selected is considered as a theoretical lower limit.

On the other hand, P_1 is set as the system's highest pressure for a cycle operating with the inert ideal gas A or A_2 for all the considered theoretical reactive gases, as presented in Eq. (34).

$$P_1 = P_{1,inert} = r_p \times P_{2,inert} \quad (34)$$

Where r_p is the pressure ratio corresponding to the inert ideal gases. In this study, a pressure ratio of $r_p = 2.72$ is considered, where it has been demonstrated by Wolgemuth [37] that this ratio produces the maximum work per unit maximum cylinder volume for any inert ideal gas.

Another condition constraining the selection of operating parameters is to ensure that the system functions as a thermal engine rather than a heat pump. In other words, the system's highest pressure P_1 should be greater than P_2, which is calculated using Eq. (24) and is a function of P_3 and the cycle temperatures (T_H and T_C). For the considered operating temperatures, increasing P_3 further leads to an infeasible operation of the reactive Stirling engine where the system operates as a heat pump.

Note that all the calculations of this study are carried out using Fortran and MATLAB codes developed by the authors.

3. Results and discussion

This section presents the results obtained for the system and operating conditions presented in Section 2.3. The behavior of a chemically reactive fluid in the Stirling cycle is investigated during isothermal expansion, isochoric cooling, isothermal compression, and isochoric heating. In addition, the work and heat quantities, and cycle performance are discussed. Whenever possible, these properties are compared to those of inert fluids A and A_2.

As aforementioned in Section 2.3, the system's lowest pressure, P_3, and highest pressure, P_1, are defined. On the other hand, the system's unknown pressures, P_2 and P_4, are calculated using Eq. (23), as presented in Fig. 2.

Note that the colormaps in this work present properties of the theoretical working fluids, that are characterized by the reaction coordinates ($\Delta_R S^\circ, \Delta_R H^\circ$) and the chemical reaction in Eq. (2). Therefore, each point on the colormap corresponds to a unique theoretical working fluid. The top-left and bottom-right regions of the colormaps correspond to inert-behaving fluids, respectively depicting pure inert fluids A_2 and A, and are used as a benchmark to assess the behavior of chemically reactive working fluids. For these fluids, the internal regeneration process remains complete, satisfying the equation $q_{23} = q_{41} = q_{reg}$, for all operating conditions.

Observing Fig. 2, for inert fluids A and A_2, P_2 amounts to 0.225 bar. However, for the majority of reactive fluids, P_2 is higher than that corresponding to the inert fluids, reaching up to 0.45 bar for high values of the reaction coordinates ($\Delta_R S^\circ, \Delta_R H^\circ$), leading to a lower expansion ratio. Exceptionally, for low values of $\Delta_R S^\circ$ and $\Delta_R H^\circ$ the calculated P_2 is lower than that of inert fluids A and A_2, yielding higher expansion ratios for the corresponding reactive fluids.

On the other hand, for A and A_2, P_4 amounts to 0.272 bar. For the majority of the reactive fluids, P_4 is lower, reaching a minimum of 0.14 bar for high values of the reaction coordinates. This indicates a lower compression ratio, compared to inert fluids. Contrarily, for low values of the reaction coordinates, the calculated P_4 is higher than that of A and A_2, yielding higher compression ratios for the corresponding reactive fluids.

3.1. Isothermal expansion: Transformation (1–2)

The equilibrium molar composition at the inlet to the isothermal expansion process ($z_{A_2,1}$), variation in the total number of moles during expansion ($\Delta n_{1-2} = n_2 - n_1$), specific heat supplied (q_{exp}), and specific work generated (w_{exp}) are presented in Fig. 3.

Observing Fig. 3(a), for low values of $\Delta_R S^\circ$ and high values of $\Delta_R H^\circ$, the fluid is purely composed of molecule A_2 at thermodynamic point (1);

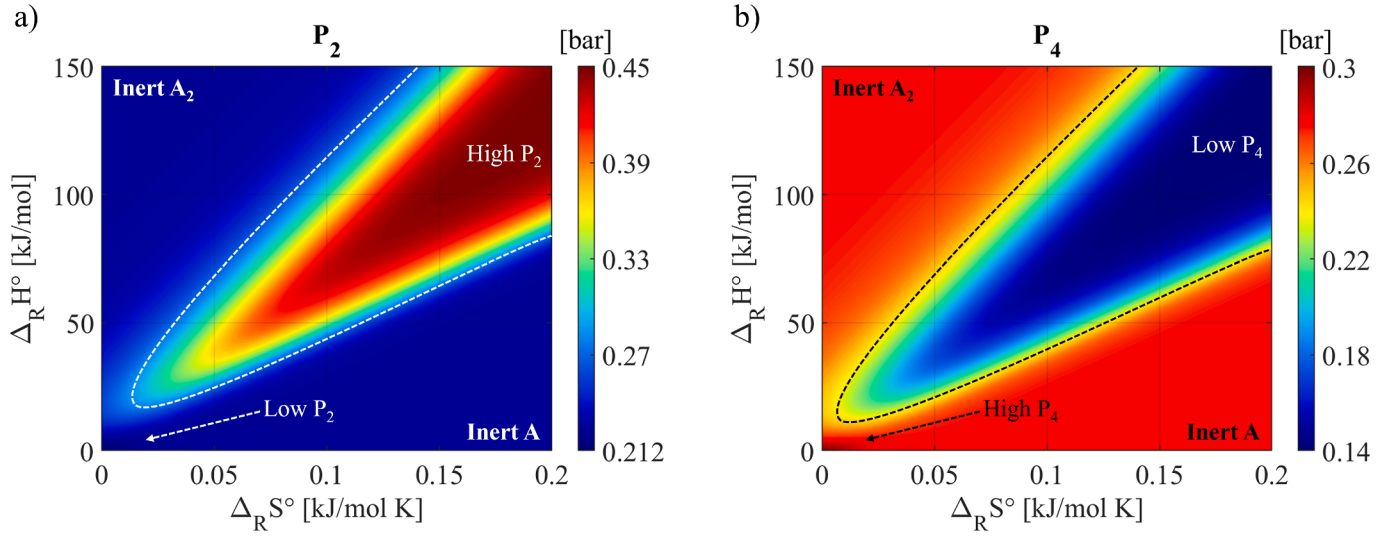

Fig.2. Cycle calculated pressures for all the studied theoretical gaseous mixtures characterized by the reaction coordinates ($\Delta_R S^\circ, \Delta_R H^\circ$) and equilibrated chemical reaction $A_{2(g)} \rightleftarrows 2A_{(g)}$. (a) Pressure at the inlet to the isochoric cooling process, P_2. (b) Pressure at the inlet to the isochoric heating process, P_4.

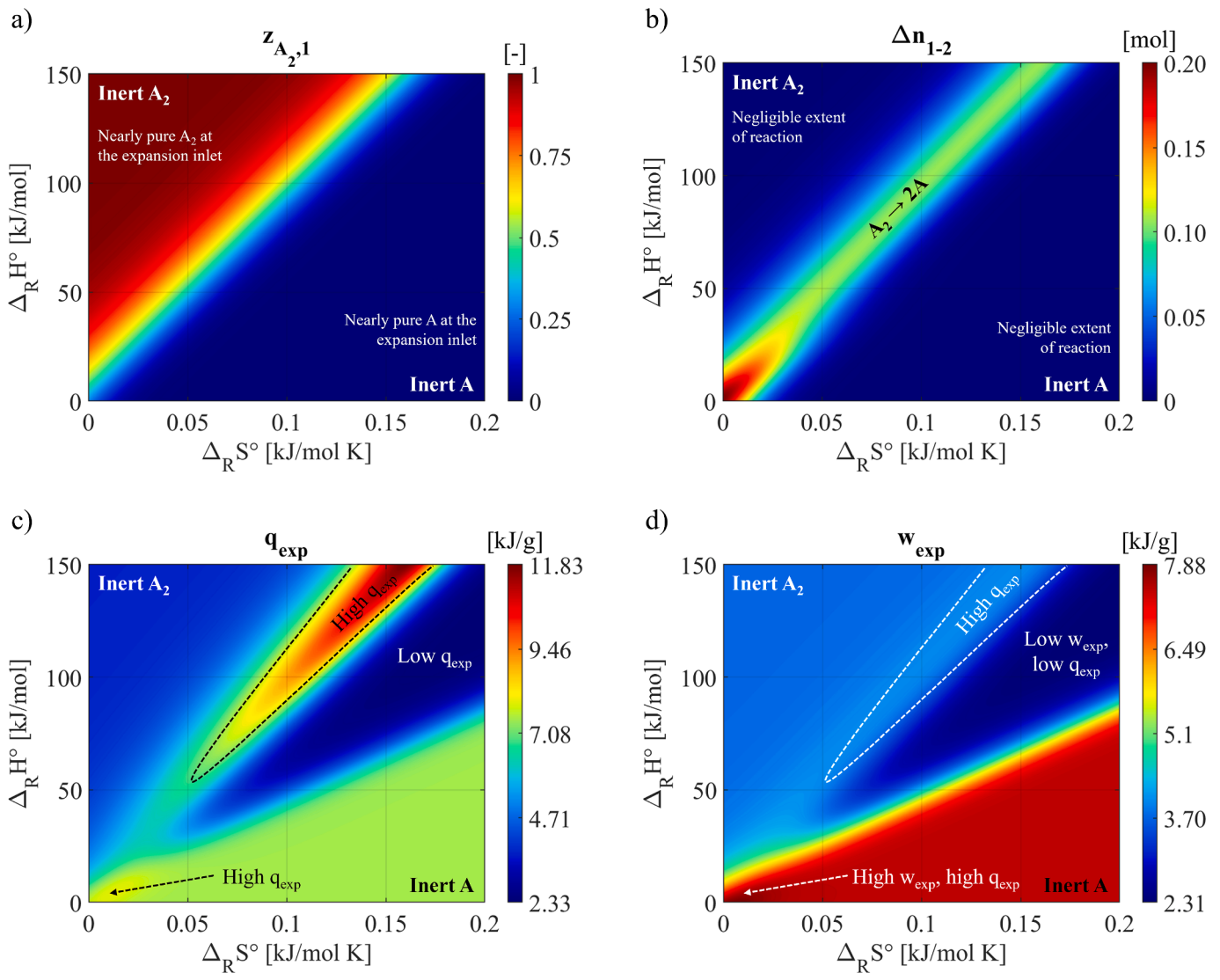

Fig.3. Behavior of the theoretical gaseous mixture, $A_{2(g)} \rightleftarrows 2A_{(g)}$, for different reaction coordinates $(\Delta_R S°, \Delta_R H°)$ during isothermal expansion (process 1 → 2). (a) Equilibrium molar fraction of molecule A_2 at the inlet to the isothermal expansion process, $z_{A_2,1}$. (b) Variation in the total number of moles during expansion, $\Delta n_{1-2} = n_2 - n_1$. (c) Specific heat input during isothermal expansion, q_{exp}. (d) Specific expansion work generated, w_{exp}.

contrarily, for high values of $\Delta_R S°$ and low values of $\Delta_R H°$, the fluid is purely composed of *A*. However, for intermediate values of $\Delta_R S°$ and $\Delta_R H°$, the equilibrium composition of the fluid becomes highly sensitive to these coordinates.

As presented in Fig. 3(b), reactive fluids undergo an increase in the total number of moles during expansion. Therefore, the reaction shifts in the endothermic dissociation direction: $A_{2(g)} \rightarrow 2A_{(g)}$. This is due to the pressure drop, at a constant temperature T_H, during expansion. According to the law of mass action, for chemically reactive working fluids, as the system's pressure decreases at a constant temperature, the chemical reaction shifts towards the increasing number of moles (dissociation reaction). For low values of $\Delta_R S°$ and $\Delta_R H°$, the variation in the total number of moles becomes more significant. This is contrary to what was observed by the authors for isentropic expansion [41,42]. Unlike isothermal expansion, for the majority of reactive fluids, the reaction shifts in the direction of the decreasing number of moles, $2A_{(g)} \rightarrow A_{2(g)}$, as both the temperature and pressure decrease during isentropic expansion. Hence, the temperature effect was observed to be more prominent in isentropic expansion than the pressure effect.

As for the expansion heat externally supplied between thermodynamic points (1) and (2), the latter amounts to 7.49 kJ/g for inert fluid *A* and 3.74 kJ/g for A_2. For reactive fluids, q_{exp} ranges from 2.33 kJ/g to 11.83 kJ/g, as presented in Fig. 3(c). As observed in Fig. 2, for the majority of the reactive fluids, the expansion outlet pressure is higher, whereas the expansion ratio is lower, compared to inert fluids *A* and A_2. Therefore, low q_{exp} values are expected for the majority of reactive fluids. However, the endothermic reaction in the fluid has an opposite effect, elevating the value of q_{exp} during isothermal expansion. This can be observed by comparing Fig. 3(b) and 3(c) where the pronounced endothermic reaction leads to higher values of q_{exp} compared to inert fluids.

Similarly, due to the lower expansion ratios, the majority of reactive fluids are expected to generate a lower expansion work compared to inert fluids *A* and A_2. However, the fluids that are characterized by a pronounced endothermic dissociation reaction yield a moderate expansion work. This is due to the transformation from complex molecules to simpler ones, *A*, due to the chemical reaction, contributing to the expansion work output. For inert ideal gases, the specific work and heat quantities are equivalent for a reversible isothermal process. Therefore, the specific expansion work generated amounts to 7.49 kJ/g for *A* and 3.74 kJ/g for A_2. Some of the reactive fluids–that are characterized by low values of the reaction coordinates–generate high w_{exp}

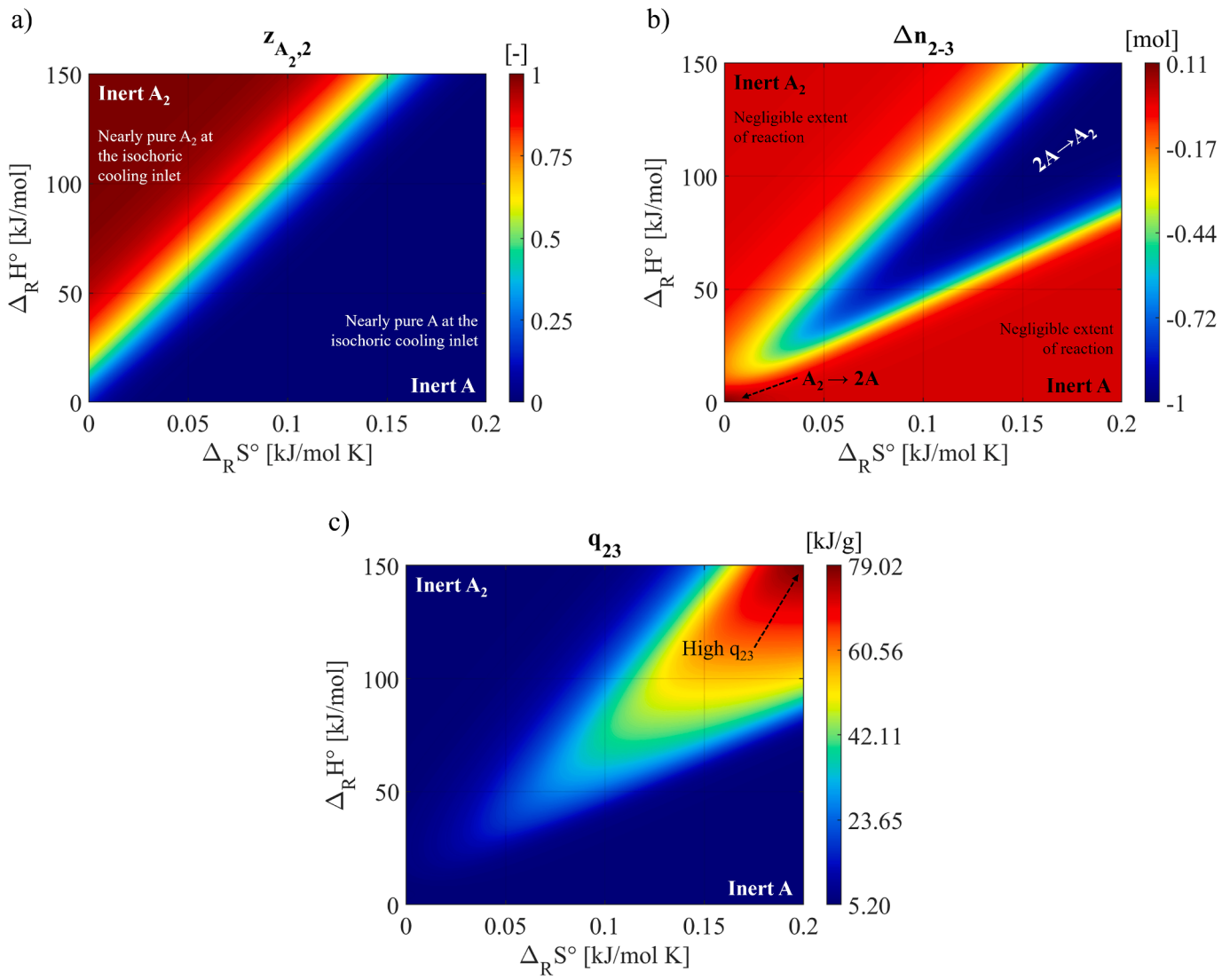

Fig.4. Behavior of the theoretical gaseous mixture, $A_{2(g)} \rightleftarrows 2A_{(g)}$, for different reaction coordinates $(\Delta_R S°, \Delta_R H°)$ during isochoric cooling (process 2 → 3). (a) Equilibrium molar fraction of molecule A_2 at the inlet to the isochoric cooling process, $z_{A_2,2}$. (b) Variation in the total number of moles during isochoric cooling, $\Delta n_{2-3} = n_3 - n_2$. (c) Total specific heat released, q_{23}.

reaching 7.88 kJ/g (around 5 % increase in w_{exp} compared to pure inert A). It can be observed that this high-w_{net} region is characterized by the most vigorous reaction shift (increase in the number of moles) compared to other reactive fluids, as well as high expansion ratios (Fig. 2).

Note that, although the reaction shifts in the opposite direction (exothermic association) in the case of isentropic expansion, the chemical reaction also positively contributes to the expansion work output [41,42]. In that case, the exothermic reaction produces a favorable reheating effect in the fluid during expansion.

3.2. Isochoric cooling: Transformation (2–3)

The equilibrium molar composition at the inlet to the isochoric cooling process $(z_{A_2,2})$, variation in the total number of moles $(\Delta n_{2-3} = n_3 - n_2)$, and the total specific heat released (q_{23}) are presented in Fig. 4.

Similar to the isothermal expansion process, the theoretical fluid is solely composed of ideal gas A for high values of $\Delta_R S°$ and low values of $\Delta_R H°$, and A_2 for low values of $\Delta_R S°$ and high values of $\Delta_R H°$ at thermodynamic state (2). The molar composition becomes sensitive to $\Delta_R S°$ and $\Delta_R H°$ at intermediate values. As presented in Fig. 4(b), the majority of reactive fluids undergo a decrease in the total number of moles during the isochoric cooling process. Therefore, the reaction shifts in the exothermic association direction: $2A_{(g)} \rightarrow A_{2(g)}$. This is not favorable for the cooling process since the exothermic reaction tends to heat the fluid. Exceptionally, for very low values of $\Delta_R S°$ and $\Delta_R H°$ the reaction shifts in the endothermic dissociation direction: $A_{2(g)} \rightarrow 2A_{(g)}$. During isochoric cooling, the temperature decreases from T_H to T_C, similarly, the pressure decreases from P_2 to P_3. Stated by the Van't Hoff equation, as the system's temperature decreases at a constant pressure, the reaction shifts in the exothermic direction. However, according to the law of mass action, as the pressure decreases at a constant temperature, the reaction shifts in the direction of increasing number of moles (endothermic direction). Therefore, the effects of temperature and pressure change during isochoric cooling are in opposition. For low values of $\Delta_R S°$ and $\Delta_R H°$, the pressure effect is more pronounced whereas for higher values of the reaction coordinates, the temperature effect becomes more pronounced. The total specific heat released in Fig. 4(c) is analogous to the variation in the total number of moles in Fig. 4(b). Higher values of q_{23} are obtained as the reaction shifts more towards the exothermic direction reaching 79.02 kJ/g for high values of $\Delta_R S°$ and $\Delta_R H°$. This signifies an increase in q_{23} up to 12.7 times compared to A and 15.2 times compared

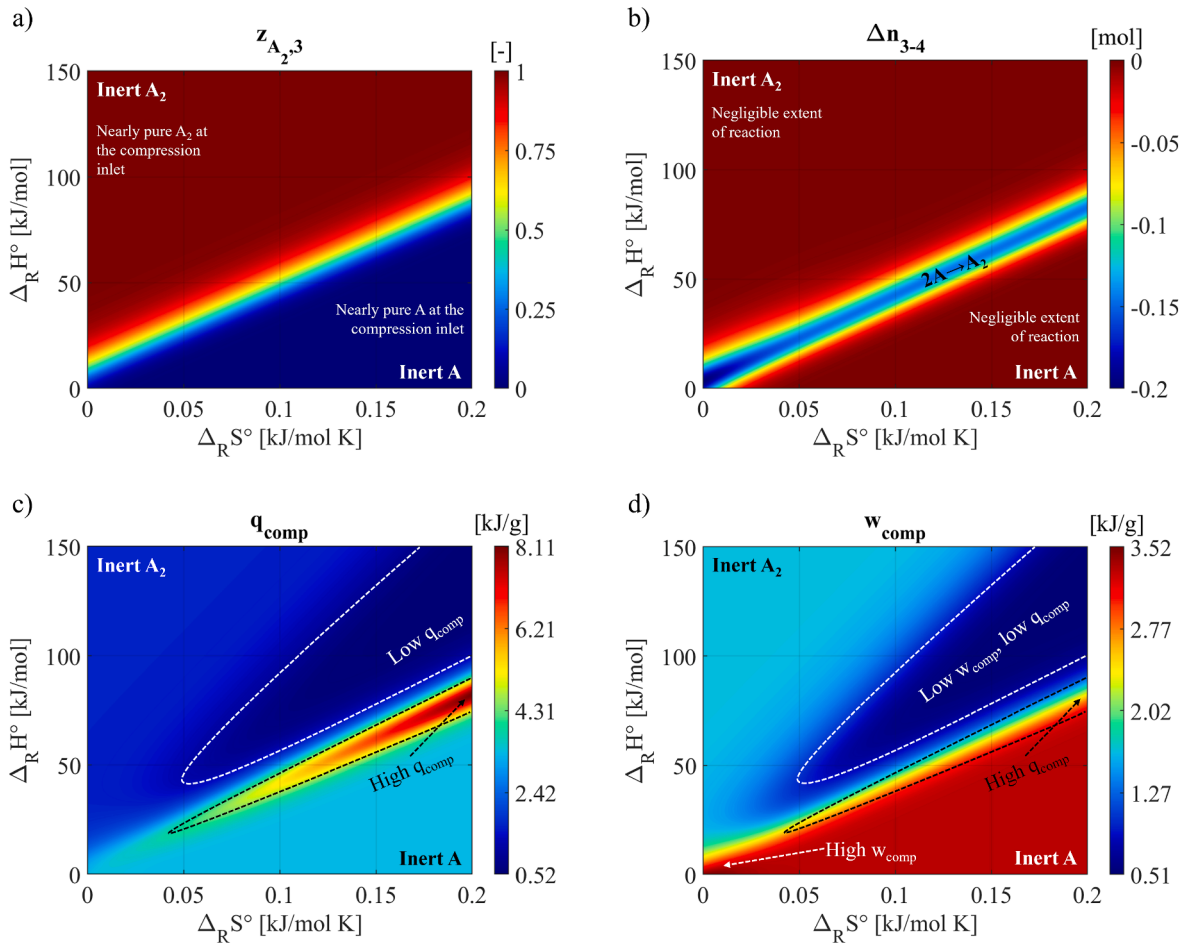

Fig.5. Behavior of the theoretical gaseous mixture, $A_{2(g)} \rightleftarrows 2A_{(g)}$, for different reaction coordinates $(\Delta_R S°, \Delta_R H°)$ during isothermal compression (process 3 → 4). (a) Equilibrium molar fraction of molecule A_2 at the inlet to the isothermal compression process, $z_{A_2,3}$. (b) Variation in the total number of moles during compression, $\Delta n_{3-4} = n_4 - n_3$. (c) Specific heat rejected during isothermal compression, q_{comp}. (d) Specific compression work input, w_{comp}.

to A_2. The latter has an implication on the internal regenerator design and the needed heat transfer surface area.

3.3. Isothermal compression: Transformation (3–4)

The equilibrium molar composition at the inlet to the isothermal compression process $(z_{A_2,3})$, variation in the total number of moles during compression $(\Delta n_{3-4} = n_4 - n_3)$, specific heat rejected (q_{comp}), and specific work input (w_{comp}) are presented in Fig. 5.

Observing Fig. 5(a), at the inlet to the isothermal compression process, the fluid is solely composed of ideal gas A for high values of $\Delta_R S°$ and low values of $\Delta_R H°$, and A_2 for low values of $\Delta_R S°$ and high values of $\Delta_R H°$. This equilibrium composition becomes highly sensitive to $\Delta_R S°$ and $\Delta_R H°$ at intermediate values. As presented in Fig. 5(b), for reactive fluids, the total number of moles decreases during isothermal compression $(\Delta n_{3-4} < 0)$. Therefore, the reaction shifts in the association exothermic direction: $2A_{(g)} \rightarrow A_{2(g)}$, conforming to the law of mass action. The reaction shift becomes more prominent for low values of the reaction coordinates $(\Delta_R S°, \Delta_R H°)$. This is contrary to what was observed in the case of isentropic–rather than isothermal–compression, where the reaction shifts towards the increasing number of moles (endothermic reaction) for the majority of reactive fluids [41,42].

Recalling Fig. 2, as a result of the chemical reaction, the compression ratio for the majority of reactive fluids is smaller than that of inert fluids A and A_2. Therefore, the specific heat released during isothermal compression, as well as the specific work input, are expected to be low. However, the exothermic effect of the reaction unfavorably increases q_{comp} where the reaction is pronounced. This can be observed by comparing Fig. 5(b) and 5(c). Therefore, for reactive fluids, q_{comp} ranges from 0.52 kJ/g to 8.11 kJ/g. Observing Fig. 5(d), w_{comp} amounts to 3.33 kJ/g for A and 1.66 kJ/g for A_2. On the other hand, it can be observed that the high w_{exp} region (Fig. 3) is also characterized by a high w_{comp}. This is due to the high compression ratio of the respective fluids.

Note that, in the case of isentropic compression, the endothermic chemical reaction positively impacts the compression work for the majority of reactive fluids by producing an intercooling effect in the fluid during compression [41,42].

3.4. Isochoric heating: Transformation (4–1)

The equilibrium molar composition at the inlet to the isochoric heating process $(z_{A_2,4})$, variation in the total number of moles $(\Delta n_{4-1} = n_1 - n_4)$, and total specific heat absorbed (q_{41}) are presented in Fig. 6.

At the inlet to the isochoric heating process, the equilibrium composition of the working fluid is similar to that at the inlet to the isothermal compression process. Observing Fig. 6(b), for the majority of the reactive wokring fluids, the total number of moles in the system increases during isochoric heating $(\Delta n_{4-1} > 0)$. Therefore, the reaction shifts in the dissociation endothermic direction: $A_{2(g)} \rightarrow 2A_{(g)}$ (unfavorable for the heating process). This justifies the relatively high values of q_{41} for the majority of reactive fluids compared to inert fluids A and A_2, reaching a maximum of 78.6 kJ/g. However, exceptionally, for low

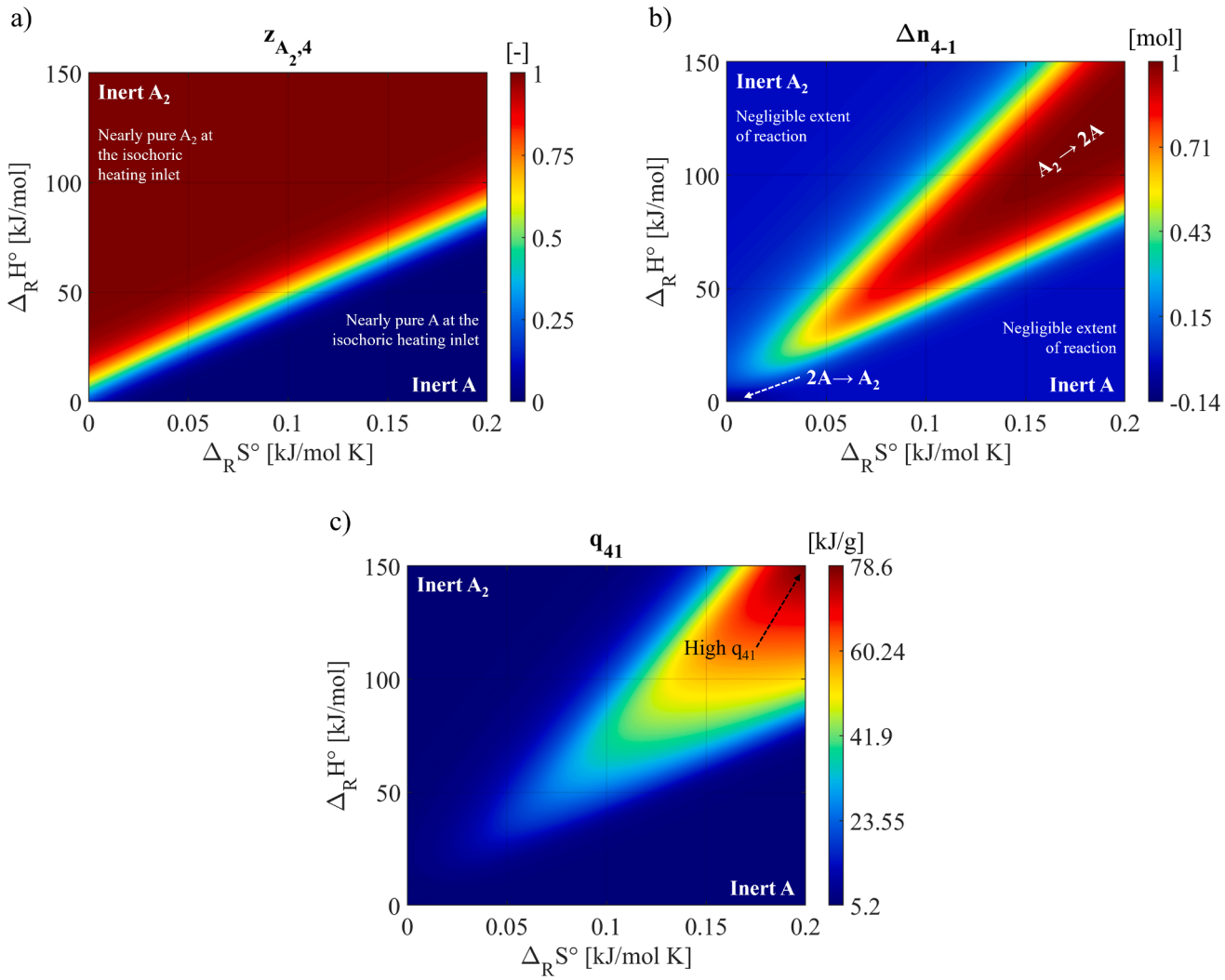

Fig.6. Behavior of the theoretical gaseous mixture, $A_{2(g)} \rightleftarrows 2A_{(g)}$, for different reaction coordinates $(\Delta_R S°, \Delta_R H°)$ during isochoric heating (process 4 → 1). (a) Equilibrium molar fraction of molecule A_2 at the inlet to the isochoric heating process, $z_{A_2,4}$. (b) Variation in the total number of moles during isochoric heating, $\Delta n_{4-1} = n_1 - n_4$. (c) Total specific heat absorbed, q_{41}.

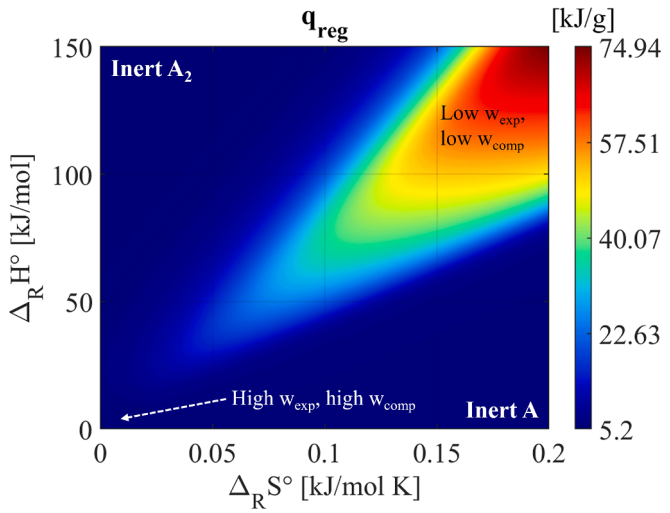

Fig.7. The specific heat exchanged in the internal regenerator between the hot (2–3) and cold (4–1) streams for each theoretical reactive fluid $A_{2(g)} \rightleftarrows 2A_{(g)} - (\Delta_R S°, \Delta_R H°)$. This heat is stored in the regenerator during isochoric cooling and reabsorbed from the regenerator during isochoric heating.

values of $\Delta_R S°$ and $\Delta_R H°$, the reaction shifts in the opposite diection, $2A_{(g)} \rightarrow A_{2(g)}$, which is an exothermic reaction.

The colormaps of q_{23} and q_{41}, respectively presented in Fig. 4(c) and 6(c), correspond to the total heat exchanged during isochoric processes (2–3) and (4–1). Alternatively, the heat transferred from the hot stream (2–3) to the cold stream (4–1) by the means of the internal regenerator for each of the reactive fluids considered is presented in Fig. 7.

The total heat rejected during isochoric cooling, total heat absorbed during isochoric heating, and the heat exchanged in the regenerator between the two streams are equivalent in the case of inert ideal gases *A* and A_2. For *A*, the two streams exchange 6.23 kJ/g in the regenerator, whereas, for A_2 this heat amounts to 5.2 kJ/g. For the majority of reactive fluids, the heat exchanged internally in the regenerator is significantly higher compared to *A* and A_2, reaching approximately 75 kJ/g for high values of the reaction coordinates $(\Delta_R S°, \Delta_R H°)$, as presented in Fig. 7. However, for the region of reactive fluids that is characterized by an enhanced expansion specific work compared to inert fluids, the heat exchanged in the regenerator is comparable to that of inert fluid *A*.

Unlike inert fluids, reactive fluids are not characterized by complete internal regeneration. As detailed in Section 2.3, incomplete regeneration can occur in three cases due to reactive fluids. Fig. 8(a) presents the fraction of the total heat released during isochoric cooling that is

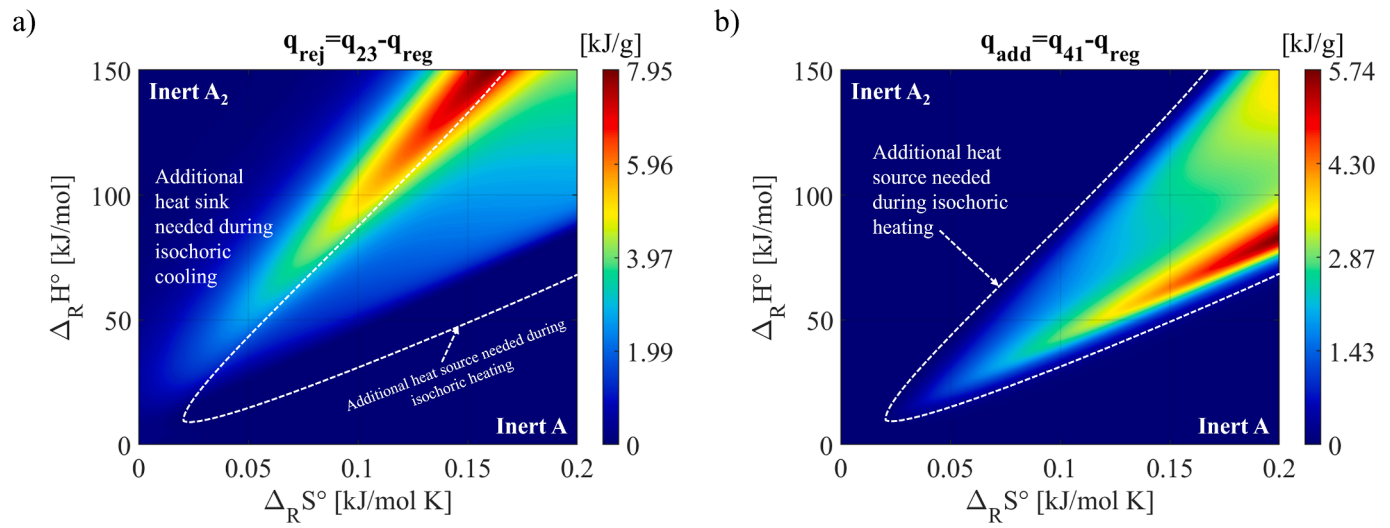

Fig.8. (a) The specific heat released out of the cycle during isochoric cooling into an additional heat sink, $q_{23} - q_{reg}$. (b) The specific heat absorbed into the cycle from an external additional heat source during isochoric heating, $q_{41} - q_{reg}$.

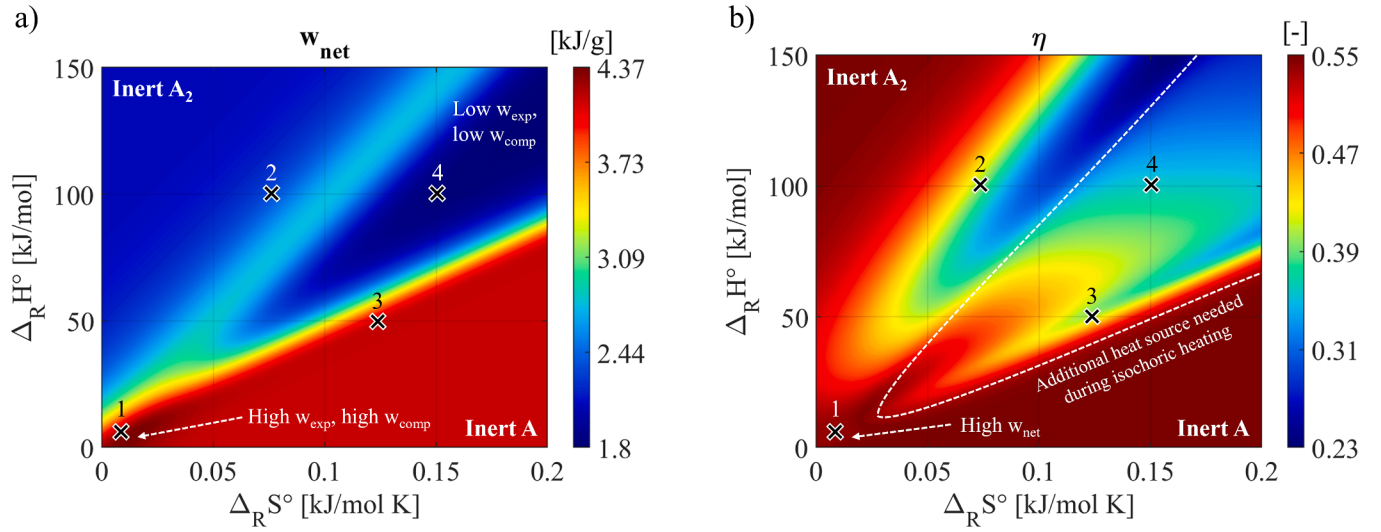

Fig.9. Overall performance of the Stirling cycle operating with theoretical ideal gas mixture $A_{2(g)} \rightleftarrows 2A_{(g)}$ for different reaction coordinates $(\Delta_R S°, \Delta_R H°)$. (a) Net specific work output, w_{net}. (b) Thermal efficiency, η. Four chemically reactive fluids are marked for further T-q diagram analysis.

released out of the cycle into an additional heat sink $\left(q_{23} - q_{reg}\right)$. Similarly, Fig. 8(b) demonstrates the fraction of q_{41} that is externally absorbed from an additional heat source $\left(q_{41} - q_{reg}\right)$, supplementing the heat absorbed from the internal regenerator, q_{reg}.

3.5. Overall cycle performance

The net specific work output w_{net} and thermal efficiency η can be calculated using Eqs. (27) and (32), as presented in Fig. 9.

Observing Fig. 9(a), the net specific work generated by the cycle amounts to 4.16 kJ/g when utilizing inert gas A as the working fluid, and 2.08 kJ/g when utilizing A_2. Due to its higher molecular complexity and weight, A_2 proves to be more suitable in the compression process, compared to A. Indeed, the compression work required for a cycle operating with A_2 is half that for a cycle operating with A. However, A proves to be more suitable in the expansion process than A_2, where the expansion work generated by an A cycle is double that generated by an A_2 cycle. On the other hand, for reactive fluids, w_{net} ranges from 1.8 kJ/g (56.7 % and 13.5 % decrease compared to A and A_2, respectively) to 4.37 kJ/g (5 % and 110 % increase compared to A and A_2, respectively) depending on the reaction coordinates $(\Delta_R S°, \Delta_R H°)$. Comparing Fig. 9 (a) and Fig. 9(b), the reactive fluids that yield improved values of w_{net} are characterized by a thermal efficiency, η, that is comparable to that of A and A_2. This substantial increase in w_{net} for low values of the reaction coordinates $(\Delta_R S°, \Delta_R H°)$, compared to inert fluid A_2, is in line with the results obtained by Walker [39] and Wolgemuth [37] for dinitrogen tetroxide.

On the other hand, according to Fig. 9(b), the thermal efficiency of an inert ideal Stirling engine is only dependent on the system's temperatures (T_C and T_H) and can be expressed as per the equation below.

$$\eta_{inert} = 1 - \frac{T_C}{T_H} \tag{35}$$

Therefore, given the system operating conditions, the thermal efficiency of a Stirling engine operating between $T_C = 400$ K and $T_H = 900$ K, with A or A_2 as the working fluid, amounts to 55.5 %. This is equivalent to the efficiency achievable by a Carnot engine operating between the same heat sink and source and represents the upper limit of

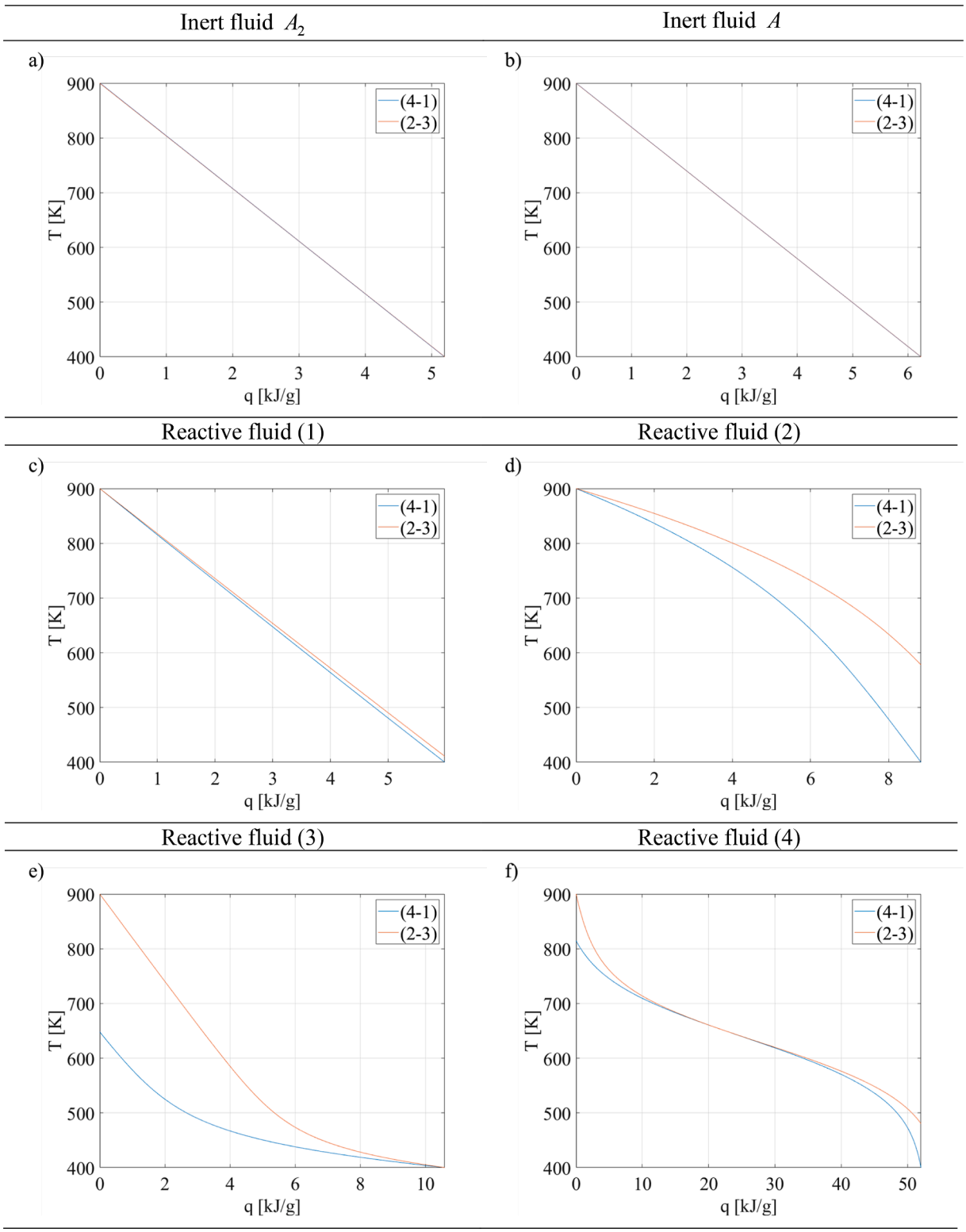

Fig.10. T-q diagrams of six theoretical working fluids: two corresponding to inert fluids A_2 (a) and A (b), and four corresponding to selected chemically reactive fluids (c-f). These fluids are identified and numbered on the w_{net} and η colormaps presented in Fig. 9.

efficiency for any chemically reactive Stirling engine, as presented in Fig. 9(b). Thus, for the theoretical reactive fluids considered in this study, η ranges from 23.4 % to 55.5 %.

In order to better understand the effect of fluids' reactivity on the heat exchange in the internal regenerator, the T-q diagrams of four reactive fluids, identified and numbered on the w_{net} and η colormaps, are plotted in Fig. 10. The T-q diagrams for inert fluids A_2 (Fig. a) and A (Fig. b) are included for reference.

Observing Fig. 10, it can be concluded that the internal regenerator is ideal in the case of inert fluids A_2 and A, where the two streams remain at the same temperature during the heat exchange. However, that is not true for reactive fluids (Fig. 10(c) through 10(f)), where heat is exchanged across a finite temperature difference. In the case of reactive fluids (1) and (2), the total heat rejected during isochoric cooling is

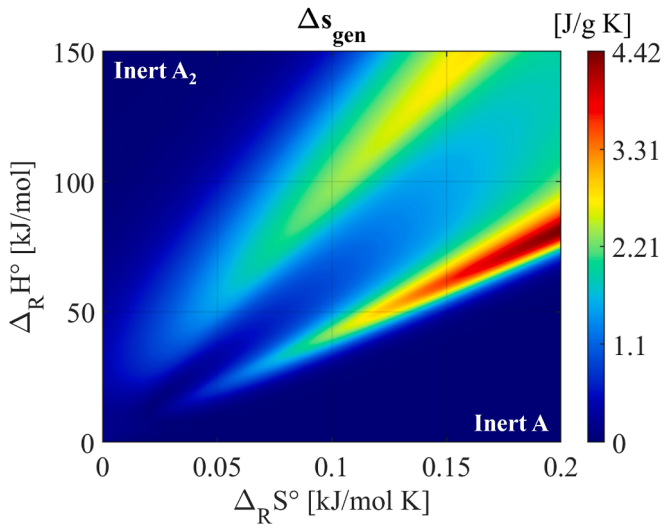

Fig.11. Specific entropy generated in the regenerator for the theoretical reactive working fluids considered, Δs_{gen}.

greater than that absorbed during isochoric heating. Therefore, in the internal regenerator, the hot stream (2–3) does not reach T_C at the end of the regenerative heat exchange, resulting in the necessity for an external heat sink during (2–3). The T-q diagram corresponding to reactive fluid (1), that yields an improved w_{net}, resembles that of an inert fluid. Contrarily, for reactive fluid (3), the total heat absorbed during isochoric heating is greater than that rejected during isochoric cooling. Thus, at the end of heat exchange in the internal regenerator, the temperature of the cold stream does not reach T_H, and an additional external heat source is needed during (4–1). On the other hand, for reactive fluid (4), the total heat rejected and absorbed during the isochoric processes are comparable. However, as shown in Fig. 10(f), both an external heat sink and heat source are needed during isochoric cooling and heating, respectively.

Therefore, the effect of the heat rejected and added externally during the isochoric processes can be observed in the T-q diagrams (Figs. c through f). As these quantities increase, the temperature difference between the two streams in the regenerator becomes more prominent, generating entropy during heat exchange. By comparing Fig. 9 (b) and Fig. 11, it can be observed that the reduced thermal efficiency for the majority of the reactive fluids, as presented in Fig. 9(b), can be partially attributed to the entropy generation in the regenerator. Lowest COP fluids in Fig. 9(b) do not correspond to fluids leading to highest generated entropy; indeed, the reduction of COP is also related to the incompleteness (or non-adiabaticity) of the regenerator (observed in Fig. 8).

Fig. 13 presents the P-v and T-s diagrams for reactive working fluid (1), which demonstrates an enhancement in the net specific work output. The P-v and T-s diagrams of inert fluids A_2 and A are presented in Fig. 12 for reference. The pressure values, net specific work output, and efficiency of these fluids are listed in Table 3.

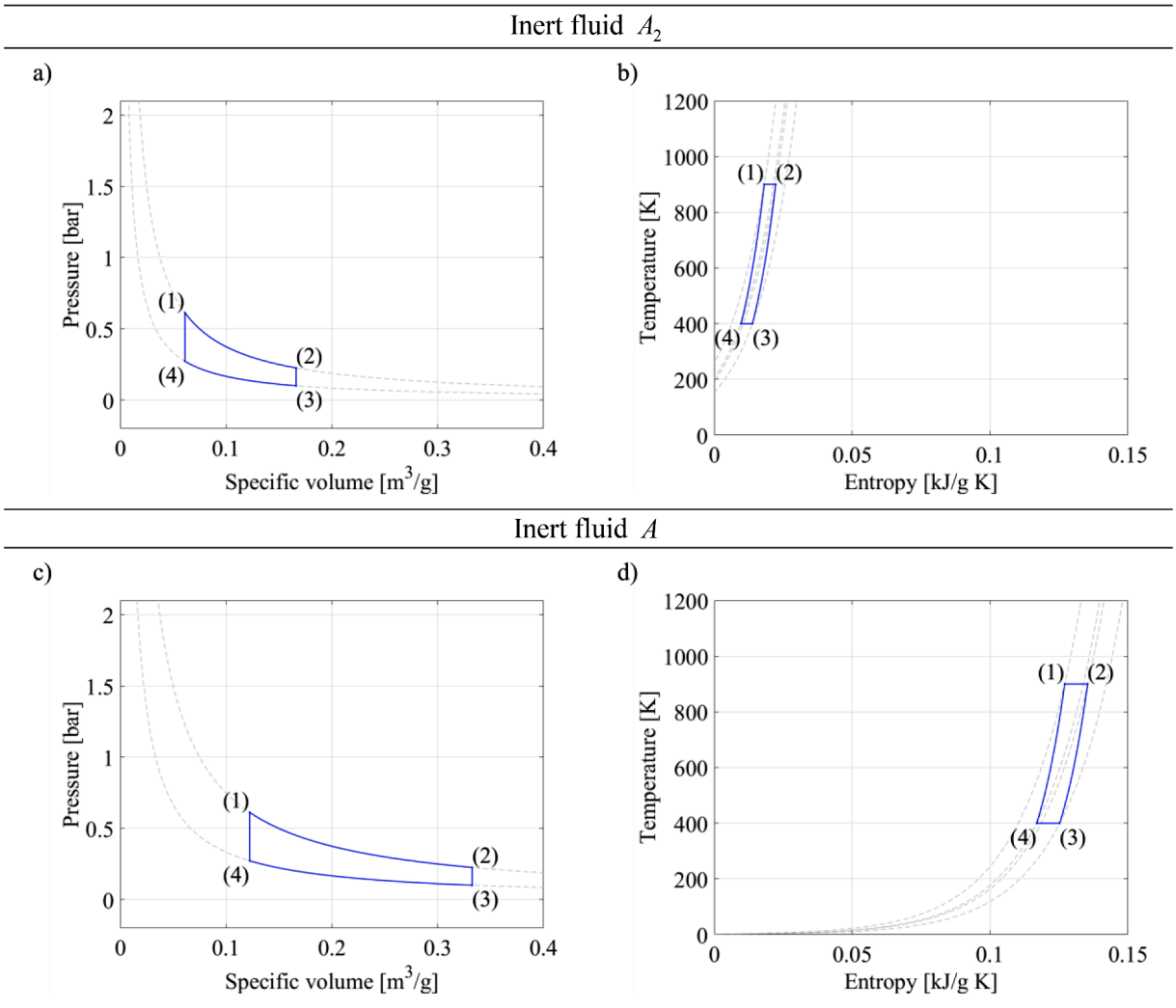

Fig.12. P-v (a) and T-s (b) diagrams of inert fluid A_2. P-v (c) and T-s (d) diagrams of inert fluid A.

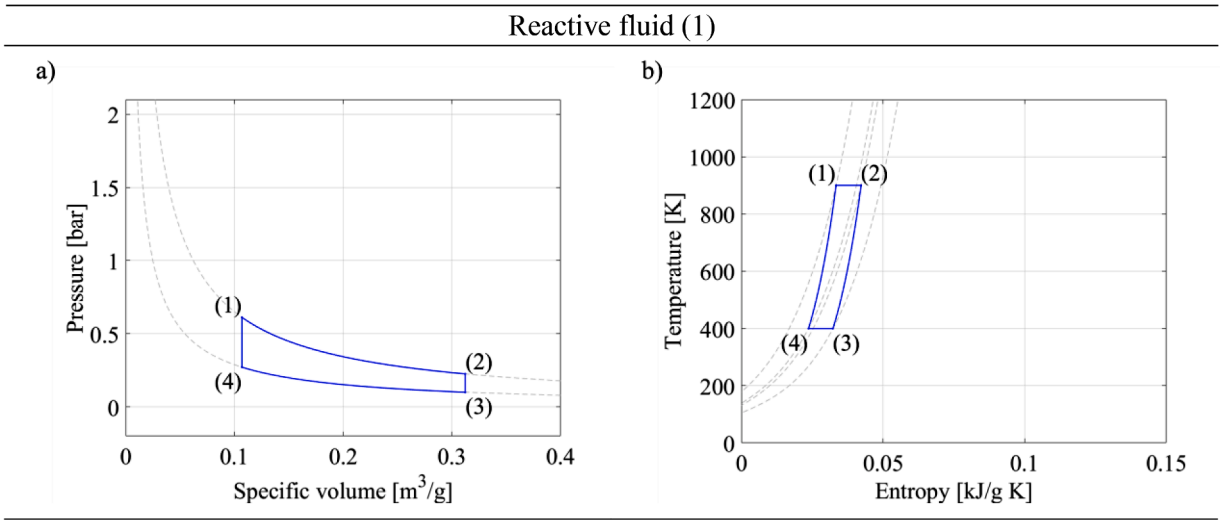

Fig.13. P-v (a) and T-s (b) diagrams of a selected reactive theoretical fluid, reactive fluid (1).

Table 3
Pressure values, net specific work output, and thermal efficiency corresponding to inert fluids A_2 and A, as well as reactive fluid (1) which demonstrates an increase in w_{net} yet a slight decrease in η.

Fluid	$\Delta_R S^\circ$ [kJ/mol K]	$\Delta_R H^\circ$ [kJ/mol]	P_2 [bar]	P_4 [bar]	w_{net} [kJ/g]	η [%]
Inert fluid A_2	0	150	0.225	0.272	2.08	55.55
Inert fluid A	0.2	0	0.225	0.272	4.16	55.55
Reactive fluid (1)	0.015	5	0.225	0.271	4.37	55.0

When assessing the net specific work output of a Stirling cycle operating with different gaseous mixtures, the area enclosed by the process curve can be compared. Observing Figs. 12 and 13, it can be deduced that the net specific work of inert fluid A is higher than that of A_2, and the selected reactive fluid achieves the highest net specific work output among the three fluids (5 % increase in w_{net} compared to A). For the selected reactive fluid, P_2 and P_4 are comparable to that of A, while P_1 and P_3 are fixed for both fluids.

4. Conclusion

This work assesses the behavior and performance of chemically reactive gases as working fluids in a Stirling engine. Unlike previous studies, which exclusively focused on the unviable dinitrogen tetroxide as a reactive working fluid in the Stirling engine, revealing significant discrepancies concerning the effect of chemical reactions on the cycle performance, this work explores a wide range of theoretical reactive working fluids. These fluids, based on equilibrated chemical reactions, are investigated using the ideal gas mixture thermodynamic model for a preliminary set of operating conditions.

The cycle's temperatures, lowest pressure, and highest pressure are fixed for all the theoretical working fluids considered. It is observed that, for reactive fluids, the internal heat exchange in the regenerator is incomplete due to variations in the specific heat capacity of the reactive fluid as the fluid's composition changes. This means that an additional heat sink during isochoric cooling, a heat source during isochoric heating, or both are required to compensate for the incomplete regeneration, penalizing the thermal efficiency of reactive Stirling engines.

Results show a maximum increase of 5 % and 110 % in w_{net} compared to inert ideal gases A and A_2, respectively. The reactive fluids that yield this increase are characterized by a comparable η to the inert fluids. They are also characterized by low values of the reaction coordinates, $(\Delta_R S^\circ, \Delta_R H^\circ)$, and the most prominent change in the number of moles during isothermal expansion and compression compared to the other reactive fluids.

However, it is observed that the Stirling engine, when operating with the majority of reactive fluids considered, undergoes a reduction in thermal efficiency. This decrease can be attributed to the incompleteness and irreversibility of the internal regenerator, where entropy is generated due to chemical reactions during the two isochoric processes.

The effect of the chemical reaction during each transformation of the Stirling engine can be summarized as follows:

1- Isothermal expansion
- The endothermic dissociation reaction during isothermal expansion transforms the fluid's composition towards simple molecules A–rather than complex molecules A_2– positively impacting the expansion work output.
- On the contrary, this endothermic reaction increases the specific heat input required during isothermal expansion.

2- Isochoric cooling
- For the majority of the reactive fluids, the reaction shifts in the direction of the decreasing number of moles during isochoric cooling (exothermic reaction). This leads to a lower expansion ratio and an increase in the heat rejected.
- Exceptionally, for low values of the reaction coordinates $(\Delta_R S^\circ, \Delta_R H^\circ)$, the reaction shifts in the opposite endothermic direction, leading to a higher expansion ratio compared to inert fluids A and A_2.

3- Isothermal compression
- During isothermal compression, the reaction shifts towards the decreasing number of moles, following the reaction $2A_{(g)} \rightarrow A_{2(g)}$, favorably reducing the compression work input.
- This exothermic reaction leads to an increase in the heat rejected to the heat sink during isothermal compression.

4- Isochoric heating
- For the majority of the reactive fluids, the reaction shifts towards the increasing number of moles during isochoric heating (endothermic reaction). This increases the heat absorbed during the process and leads to a lower compression ratio.

- Exceptionally, for low values of the reaction coordinates $(\Delta_R S^\circ, \Delta_R H^\circ)$, the reaction shifts in the opposite exothermic direction, leading to a higher compression ratio compared to that corresponding to A and A_2.

CRediT authorship contribution statement

Aya Barakat: Writing – original draft, Validation, Software, Methodology, Investigation, Conceptualization. **Silvia Lasala:** Writing – review & editing, Validation, Supervision, Methodology, Investigation, Funding acquisition, Conceptualization. **Philippe Arpentinier:** Writing – review & editing, Resources. **Pascal Tobaly:** Writing – review & editing, Conceptualization. **Jean-Noël Jaubert:** Writing – review & editing, Validation, Supervision, Investigation, Conceptualization.

Declaration of competing interest

The authors declare the following financial interests/personal relationships which may be considered as potential competing interests: Silvia Lasala reports financial support was provided by European Commission. If there are other authors, they declare that they have no known competing financial interests or personal relationships that could have appeared to influence the work reported in this paper.

Data availability

Data will be made available on request.

Acknowledgments

This work has received funding from the European Research Council (ERC) under the European Union's Horizon Europe research and innovation program (grant agreement No. 101040994).

References

[1] Laazaar K, Boutammachte N. Development of a new technique of waste heat recovery in cement plants based on Stirling engine technology. Appl Therm Eng 2022;210:118316. https://doi.org/10.1016/j.applthermaleng.2022.118316.
[2] Mahjoob Karambasti B, Ghodrat M, Ghorbani G, Lalbakhsh A, Behnia M. Design methodology and multi-objective optimization of small-scale power-water production based on integration of Stirling engine and multi-effect evaporation desalination system. Desalination 2022;526:115542. https://doi.org/10.1016/j.desal.2021.115542.
[3] Singh UR, Kumar A. Review on solar Stirling engine: development and performance. Therm Sci Eng Prog 2018;8:244–56. https://doi.org/10.1016/j.tsep.2018.08.016.
[4] Güven M, Bedir H, Anlaş G. Optimization and application of Stirling engine for waste heat recovery from a heavy-duty truck engine. Energ Conver Manage 2019;180:411–24. https://doi.org/10.1016/j.enconman.2018.10.096.
[5] Wang K, Sanders SR, Dubey S, Choo FH, Duan F. Stirling cycle engines for recovering low and moderate temperature heat: a review. Renew Sustain Energy Rev 2016;62:89–108. https://doi.org/10.1016/j.rser.2016.04.031.
[6] Nightingale NP. Automotive Stirling engine: Mod 2 design report. NAS 1.26:175106; Oct. 1986. Accessed: Apr. 25, 2023. [Online]. Available: https://ntrs.nasa.gov/citations/19880002196.
[7] Postma ND, Giessel RV, Reinink F. The Stirling engine for passenger car application. Warrendale, PA: SAE International. SAE Technical Paper 730648; Feb. 1973. doi: 10.4271/730648.
[8] van Giessel R, Reinink F. Design of the 4–215 D.A. automotive Stirling engine. SAE Trans 1977;86:319–32.
[9] Dowdy MW, Nightingale NP. Mod I automotive Stirling engine system performance. Warrendale, PA: SAE International. SAE Technical Paper 820353; Feb. 1982. doi: 10.4271/820353.
[10] Timoumi Y, Tlili I, Ben Nasrallah S. Design and performance optimization of GPU-3 Stirling engines. Energy 2008;33(7):1100–14. https://doi.org/10.1016/j.energy.2008.02.005.
[11] Ghanem CR, Gereige EN, Bou Nader WS, Mansour CJ. Stirling system optimization for series hybrid electric vehicles. Proc Inst Mech Eng, Part D: J Autom Eng 2022;236(2–3):407–23. https://doi.org/10.1177/09544070211018034.
[12] Nader WB, Mansour C, Nemer M, Dumand C. Fuel consumption saving potential of Stirling machine on series parallel hybrid electric vehicle: case of the Toyota prius. Warrendale, PA: SAE International. SAE technical paper 2018-01-0421; Apr. 2018. doi: 10.4271/2018-01-0421.
[13] Raska M. Diesel-electric submarine modernization in Asia: the role of air-independent propulsion systems. In: Bitzinger RA, editor. Emerging critical technologies and security in the Asia-Pacific. London: Palgrave Macmillan UK; 2016. p. 91–106. https://doi.org/10.1057/9781137461285_8.
[14] Thieme LG. Technology development for a Stirling radioisotope power system. In: AIP conference proceedings. Seoul, Korea: AIP; 2000. p. 1260–5. https://doi.org/10.1063/1.1290937.
[15] Wilson SD, Schifer N, Casciani MR. Small Stirling technology exploration power for future space science missions. In: 2019 IEEE aerospace conference; Mar. 2019. p. 1–5. doi: 10.1109/AERO.2019.8742222.
[16] Yang S, Liu Z. Shenzhou 15 completes all scheduled tasks in space for half a year. Int Acad Assoc Commun 2023;1(2). Accessed: Oct. 02, 2023. [Online]. Available: https://ojs.ukscip.com/index.php/iaac/article/view/162.
[17] Ahmadi MH, Sayyaadi H, Dehghani S, Hosseinzade H. Designing a solar powered Stirling heat engine based on multiple criteria: maximized thermal efficiency and power. Energ Conver Manage 2013;75:282–91. https://doi.org/10.1016/j.enconman.2013.06.025.
[18] Pavlović TM, Radonjić IS, Milosavljević DD, Pantić LS. A review of concentrating solar power plants in the world and their potential use in Serbia. Renew Sustain Energy Rev 2012;16(6):3891–902. https://doi.org/10.1016/j.rser.2012.03.042.
[19] Yaqi L, Yaling H, Weiwei W. Optimization of solar-powered Stirling heat engine with finite-time thermodynamics. Renew Energy 2011;36(1):421–7. https://doi.org/10.1016/j.renene.2010.06.037.
[20] Rogdakis ED, Antonakos GD, Koronaki IP. Thermodynamic analysis and experimental investigation of a Solo V161 Stirling cogeneration unit. Energy 2012;45(1):503–11. https://doi.org/10.1016/j.energy.2012.03.012.
[21] Aliabadi AA, Thomson M, Wallace J, Tzanetakis T, Lamont W, Carlo J. Efficiency and emissions measurement of a Stirling-engine-based residential microcogeneration system run on diesel and biodiesel. Energy & Fuels - Energ Fuel 2009;23. https://doi.org/10.1021/ef800778g.
[22] Radebaugh R. Cryocoolers: the state of the art and recent developments*. J Phys: Condens Matter 2009;21(16):164219. https://doi.org/10.1088/0953-8984/21/16/164219.
[23] Walker G, Fauvel R, Gustafson R, van Bentham J. Stirling engine heat pumps. Int J Refrig 1982;5(2):91–7. https://doi.org/10.1016/0140-7007(82)90083-4.
[24] Penswick L, Olan RW, Williford I, Draney S, Buchholz G. High-capacity and efficiency Stirling cycle cryocooler. In: Cryocoolers 18, Boulder, CO; 2014.
[25] Li X, et al. A high-efficiency free-piston Stirling cooler with 350 W cooling capacity at 80 K. Energy Proc 2019;158:4416–22. https://doi.org/10.1016/j.egypro.2019.01.775.
[26] Minkina V. Hydrogen generation and storage from sodium borohydride; 2015. p. 501–512. doi: 10.1007/978-3-319-17031-2_36.
[27] Zare S, Tavakolpour-Saleh A. Free piston Stirling engines: a review. Int J Energy Res 2020;44(7):5039–70. https://doi.org/10.1002/er.4533.
[28] Khan U, Zevenhoven R, Stougie L, Tveit T-M. Prediction of Stirling-cycle-based heat pump performance and environmental footprint with exergy analysis and LCA. Energies 2021;14(24):24. https://doi.org/10.3390/en14248478.
[29] Metwally MM, Walker G. Stirling engines with a chemically reactive working fluid—some thermodynamic effects. J Eng Power 1977;99(2):284–7. https://doi.org/10.1115/1.3446287.
[30] Swift GW. A Stirling engine with a liquid working substance. J Appl Phys 1989;65(11):4157–72. https://doi.org/10.1063/1.343321.
[31] Swift GW. Simple theory of a Malone engine. In: Proceedings of the 24th intersociety energy conversion engineering conference. Vol. 5; Aug. 1989. p. 2355–61. doi: 10.1109/IECEC.1989.74803.
[32] Swift GW. Experiments with a Malone engine. In: Proceedings of the 24th intersociety energy conversion engineering conference. Vol. 5; Aug. 1989. p. 2385–93. doi: 10.1109/IECEC.1989.74808.
[33] Walker G. Stirling cycle cooling engine with two-phase, two-component working fluid. Cryogenics 1974;14(8):459–62. https://doi.org/10.1016/0011-2275(74)90209-4.
[34] Renfroe DA. Effects of using a two-phase two-component working fluid in a Stirling engine. In: Proc Intersoc Energy Convers Eng Conf; (United States), Vol. 2, Art. no. CONF-830812; Aug. 1983. Accessed: Nov. 17, 2022. [Online]. Available: https://www.osti.gov/biblio/5477285.
[35] Renfroe DA. A computer model of a Stirling engine using a two-phase two-component working fluid. Texas A&M University; 1981. Ph.D. dissertation.
[36] Lasala S, Privat R, Jaubert J-N, Lasala S, Privat R, Jaubert J-N. Inert and reactive working fluids for closed power cycles: present knowledge. In: Intechopen; 2018. https://doi.org/10.5772/intechopen.79290.
[37] Wolgemuth CH. The use of a chemically reactive gas in a closed Stirling cycle. The Ohio State University; 1934. Ph.D. dissertation.
[38] Schmidt G. Theorie der geschlossenen calorischen Maschine von Laubroy und Schwartzkopff in Berlin. Z Ver Oster Ing 1861:79.
[39] Walker G. Stirling engines. New York, NY: Oxford University Press; 1980. Accessed: Jan. 11, 2023. [Online]. Available: https://www.osti.gov/biblio/6710046.
[40] Kovtun IM, Naumov AN, Nesterenko VB. Stirling cycle using a dissociating gas. Akademiia Navuk BSSR, Vestsi, Seryia Fizika-Tekhnichnykh Navuk 1967;1:52–7.
[41] Lasala S, Privat R, Herbinet O, Arpentinier P, Bonalumi D, Jaubert J-N. Thermo-chemical engines: unexploited high-potential energy converters. Energ Conver Manage 2021;229:113685. https://doi.org/10.1016/j.enconman.2020.113685.
[42] Barakat A, Lasala S, Arpentinier P, Jaubert J-N. The original and impactful exploitation of chemical energy in heat pumps. Chem Eng J Adv 2022;12:100400. https://doi.org/10.1016/j.ceja.2022.100400.

[43] Gheith R, Aloui F, Nasrallah SB. Study of the regenerator constituting material influence on a gamma type Stirling engine. J Mech Sci Technol 2012;26(4):1251–5. https://doi.org/10.1007/s12206-012-0218-9.
[44] Callen HB. Thermodynamics and an introduction to thermostatistics. 2nd ed. Wiley; 1985.
[45] Smith JM, Van Ness HC, Abbott MM. Introduction to chemical engineering thermodynamics. 7th ed. Vol. 27. Singapore: McGraw-Hill; 2005.
[46] Çengel YA, Boles MA, Kanoglu M. Thermodynamics: an engineering approach. 9th Ed. New York, NY: McGraw-Hill Education; 2019.
[47] Lemmon EW, Bell IH, Huber ML, McLinden MO. NIST standard reference database 23: reference fluid thermodynamic and transport properties-REFPROP. Gaithersburg: National Institute of Standards and Technology; 2018.